New Journal of Physics
The open access journal at the forefront of physics

PAPER

The ultimate state of convection: a unifying picture of very high Rayleigh numbers experiments

Philippe-E Roche

CNRS/UGA, Institut NEEL, F-38042 Grenoble, France

Abstract

The long-standing puzzle of diverging heat transport measurements at very high Rayleigh numbers (Ra) is addressed by a simple model based on well-known properties of classical boundary layers. The transition to the 'ultimate state' of convection in Rayleigh–Bénard cells is modeled as sub-critical transition controlled by the instability of large-scale boundary-layer eddies. These eddies are restricted in size either by the lateral wall or by the horizontal plates depending on the cell aspect ratio (in cylindrical cells, the cross-over occurs for a diameter-to-height ratio around 2 or 3). The large-scale wind known to settle across convection cells is assumed to have antagonist effects on the transition depending on its strength, leading to wind-immune, wind-hindered or wind-assisted routes to the ultimate regime. In particular winds of intermediate strength are assumed to hinder the transition by disrupting heat transfer, contrary to what is assumed in standard models. This phenomenological model is able to reconcile observations from more than a dozen of convection cells from Grenoble, Eugene, Trieste, Göttingen and Brno. In particular, it accounts for unexplained observations at high Ra, such as Prandtl number and aspect ratio dependences, great receptivity to details of the sidewall and differences in heat transfer efficiency between experiments.

How does natural convection transport heat in the limit of intense thermal forcing ? This old question is still vividly disputed in the convection community.

Beyond the academic motivation of unraveling the properties of natural convection in its asymptotic limit, understanding these intense flows is relevant to various environmental (oceans, . . .) and large scale industrial flows (nuclear reactors, . . .). Indeed, the intensity of forcing in natural convection is proportional to the cube of the flow vertical extension, resulting in intense forcing in large-scale flows, even when a moderate temperature difference is driving the motion.

A model system is prevalent in laboratory studies of natural convection: the Rayleigh–Bénard cell operated in Boussinesq conditions [1] (see figure 1(a)). As detailed in the next section, three dimensionless numbers traditionally characterize respectively the thermal forcing, the fluid properties and the resulting heat transfer: the Rayleigh (Ra), Prandtl (Pr) and Nusselt (Nu) numbers. This study focuses exclusively on fluids with intermediate Pr, that is fluids with comparable viscous and thermal molecular diffusivities, such as air, helium and water, and not on fluids where one diffusivity significantly exceeds the other one, such as liquid metals or oils. We refer the reader to the review [2], and references within, for a general introduction on turbulent Rayleigh–Bénard convection.

The heat transfer dependence Nu(Ra) at given Pr provides an indirect but easily measurable piece of information on the flow. Thus, most models of convection provide predictions for this dependence. In 1962, R Kraichnan predicted the existence of an asymptotic flow regime at very high Ra, characterized by the presence of turbulence not only in the bulk of the flow—as in the preceding regime—but also in its boundary layers [3]. A distinctive Nu(Ra) dependence—recalled later—was predicted by Kraichnan, with a significantly enhanced heat transport compared to the preceding flow regime called *hard turbulence* state. The first observation of a marked Nu(Ra) transition interpreted following Kraichnan's prediction was reported in Grenoble in the late 90s [4]. The expressions '*ultimate regime*' [4] or equivalently '*ultimate state*'
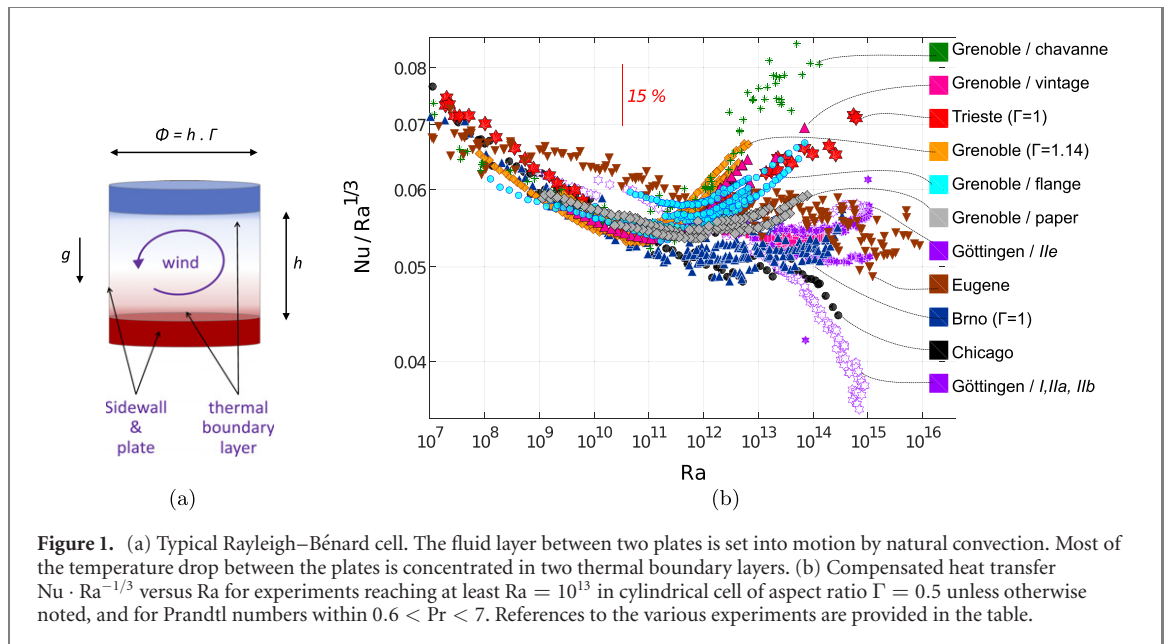
Figure 1. (a) Typical Rayleigh–Bénard cell. The fluid layer between two plates is set into motion by natural convection. Most of the temperature drop between the plates is concentrated in two thermal boundary layers. (b) Compensated heat transfer $Nu \cdot Ra^{-1/3}$ versus Ra for experiments reaching at least $Ra = 10^{13}$ in cylindrical cell of aspect ratio $\Gamma = 0.5$ unless otherwise noted, and for Prandtl numbers within $0.6 < Pr < 7$. References to the various experiments are provided in the table.

Table 1. Very high Ra Rayleigh–Bénard experiments discussed in the present paper.

Location	Aspect ratio $\Gamma = \frac{\phi}{h}$	Complementary designation	Cell height h [cm]	Fluid	Comment and references
Grenoble	0.5	*Chavanne*	20	He cryo	[4, 15]
Grenoble	0.23		43	He cryo	[16]
Grenoble	0.5	*Vintage*	20	He cryo	Reference $\Gamma = 0.5$ cell with a 1.3° or 3.6° tilt [16]
Grenoble	0.5	*Flange*	20	He cryo	With a flange at sidewall mid-height[16]
Grenoble	0.5	*Paper*	20	He cryo	With layers of paper on the inner sidewall[16]
Grenoble	0.5	*ThickWall*	20	He cryo	With sidewall x 4.4 thicker [17]
Grenoble	1.14		8.8	He cryo	[16]
Chicago	0.5		40	He cryo	[18]
Eugene	0.5		100	He cryo	[19, 20]
Trieste	1		50	He cryo	Eugene experiment moved to Trieste [21]
Trieste	4		12.5	He cryo	[22]
Brno	1		30	He cryo	[10, 23]
Göttingen	0.33		330	SF$_6$	[24]
Göttingen	0.5	I, IIa, IIb	224	SF$_6$	Unsealed [25, 92]
Göttingen	0.5	IIe	224	SF$_6$	Seals between plates and sidewall [26]
Göttingen	1		112	SF$_6$	[27]

[5] were coined at that time to name the new flow state observed at very large Ra. We choose to use the same terminology in this paper.

Since, new experiments have explored Rayleigh–Bénard convection at very high Ra (say $Ra > 10^{13}$) and for intermediate Pr, in Grenoble, Eugene, Trieste, Göttingen and Brno (see table 1 for references). As illustrated by figure 1(b), most Nu(Ra) measurements agree below $Ra \simeq 10^{11}$, while the situation at larger Ra is more puzzling and has been a fuel for scientific controversy [6–14]. Indeed, the compensated heat transfer $Nu \cdot Ra^{-1/3}$ decreases or level out with Ra in some experiments (Chicago, Eugene, Brno) while it increases significantly in others (Grenoble, Trieste), leading up to a two-fold difference in heat transfer efficiency around $Ra = 10^{14}$.

How does the convection literature deal with the striking *apparent* contradiction between the high Ra datasets? Over the years, three different approaches have consolidated in Grenoble/Lyon (e.g. see [4, 16]), Trieste/Brno/Prague (e.g. see [21, 23]) and Göttingen/Santa Barbara/Twente (e.g. see [27, 28]) to account for the results[1]. These views are either based on variants of Kraichnan's prediction or on non-Boussinesq approximation effects. Taken separately, the respective datasets and interpretations are certainly fair and often self-consistent, but no proposed model is yet able to account for all existing observations. As a consequence, most papers propose a simple discussion, but disregard or depreciate previous results in apparent contradiction.

---

[1] Surely, there are differences in judgment and emphasis between the members of the three subgroups.

It is easy to disregard experimental datasets because the ideal Rayleigh–Bénard cell, operated in perfectly Boussinesq approximation will never exist. In real life, measurements can be biased by numerous side-effects, including violations of the Boussinesq approximation, finite conductivity/response time of the heating and cooling plates, fluid property uncertainties, gas and heat leaks, etc…These effects are certainly interesting to understand, as attested by vivid arguments exchanges [7–10]. Still, it seems unrealistic to us that such effects can fully account for the 'sudden' appearance of discrepancies right above $Ra \simeq 10^{12}$ knowing that all datasets are consistent at lower Ra.

The present work explores a new and inclusive modeling approach. We first make the (subversive ?) hypothesis that all very high Ra experiments are not significantly biased by side-effects, at least not enough to fully account for a scatter of Nu(Ra) appearing above $Ra \simeq 10^{12}$. In other words, we will assume that the surprising experimental results regarding—for instance—the Nu(Ra) scatter, the unexplained aspect ratio dependence of the transition and the sensitivity to experimental details *are not problems but features of the transition to the ultimate state of convection*. An heuristic approach allows to profile a minimal model able to reconcile all the apparently 'contradictory experiments'. This model relies on three conjectures, each based on well known properties of transiting classical boundary layers[2]. These conjectures are presented in the section 2, after the introductory section 1.

1. Introduction

1.1. Dimensionless numbers

Rayleigh–Bénard cells consist in a layer of fluid confined between two horizontal plates [1], as illustrated by figure 1(a). A destabilizing temperature difference Δ is imposed between the two plates, such that natural convection motion appears in the cell. The Boussinesq approximation consists in assuming fluid incompressibility (except for a linear temperature dependence of density yielding the buoyant term), constant fluid properties, and decoupling of heat and mechanical energies [1, 29]. In this approximation, the flow is determined by only two control parameters which are traditionally chosen as the Rayleigh and Prandtl numbers. Their respective definitions are:

$$\mathrm{Ra} = \frac{\alpha \Delta h^3 g}{\kappa \nu}$$

and

$$\mathrm{Pr} = \frac{\nu}{\kappa}$$

where α, κ, ν, g and h are respectively the isobaric thermal expansion coefficient, the molecular thermal diffusivity, the kinematic viscosity, the gravitational acceleration and the cell inner height. The Rayleigh number can be seen as the control parameter associated with the thermal forcing of the flow while the Prandtl number is the only relevant property of the fluid. In this study, we only focus on Prandtl numbers of order unity (typically $0.6 \lesssim \mathrm{Pr} \lesssim 7$), which are found in air, water, helium, SF_6, perfect gases,…In response to thermal forcing, a heat flux P is transported across the cell from the hotter plate to the colder one (when $\alpha > 0$). The corresponding dimensionless number is the Nusselt number Nu, defined as

$$\mathrm{Nu} = \frac{P}{P_{\mathrm{dif}}} \tag{1}$$

where P_{dif} is the heat flux that would diffuse by molecular conduction through the cell if the fluid was quiescent. The Nusselt number can be seen as the efficiency of convection as a heat transport mechanism. In practice, Rayleigh–Bénard cells are bounded by vertical sidewalls. In cylindrical cells of diameter ϕ and height h, it results in an extra dimensionless control parameter: the cell aspect ratio Γ defined as

$$\Gamma = \frac{\Phi}{h}.$$

1.2. The hard turbulence state

The so-called *hard-turbulence state* [30] is the flow regime which precedes the ultimate one on the scale of increasing Ra. For aspect ratio and Prandtl numbers of order 1, its onset is typically around $Ra = 10^7$–10^8 [18] and its heat transfer dependence Nu(Ra) can be described with an effective local scaling $Nu \sim Ra^\gamma$ such that $2/7 \lesssim \gamma(\mathrm{Ra}) \lesssim 1/3$. Nearly all heat transfer measurements Nu(Ra, Pr) reported in the literature agree within typically a few percents over more than 4 decades of Ra, provided that second order effects and

---

[2] Here 'classical boundary layers' refers to the boundary layers of Navier–Stokes fluids.

corrections are taken into account. These effects include in particular temperature drop across the plates (eg. [31–34]), finite conductance of the sidewall (eg. [35–37]), dependence with the cell's aspect ratio (eg. [38–44]), residual tilt of the cell (e.g. [45–47]), black body radiation (eg. [48–51]), flow multistability (eg. [52–54]), adiabatic gradient correction [1, 15] and systematic errors on fluid properties.

A number of theoretical models describes the hard turbulence state (eg. see [30, 55–64]). At first order, the observed Nu(Ra) dependence can be accounted by the elegant model of W Malkus [55, 56] which predicts:

$$Nu(Ra) \sim Ra^{1/3}.$$

Malkus $\frac{1}{3}$ exponent is simply derived writing that i) the heat transfer across the cell is limited by two boundary layer resistances localized near the interface between each thermal plate and the fluid, ii) the thermal resistance of these boundary layers is independent of the cell height. The concept of quasi-independent *boundary layers* concentrating most of the temperature gradient near the plates is well accepted[3]. Most of the alternative models listed above can be seen as corrections of Malkus model that introduce some coupling between both boundary layers, for instance through a large scale circulation across the cell or by exchange of thermal plumes crossing the cell. These models allows to account for the observation of scaling exponents slightly lower than Malkus exponent $\gamma = \frac{1}{3}$. Incidentally, a $Nu \sim Ra^{(\frac{1}{3}\pm0.006)}$ scaling over nearly 3 decades of Ra can been obtained in a vertically-elongated Rayleigh–Bénard cell ($\Gamma \simeq 0.23$), suggesting that the residual coupling between boundary layers is cancelled in highly confined geometries [16].

1.3. The ultimate state of convection

At large enough Ra, R Kraichnan predicted that the boundary layers will undergo a turbulent transition, leading to a turbulent heat transfer across the boundary layers [3][4], with the following heat transfer dependence:

$$Nu(Ra) \sim \frac{Ra^{1/2}}{\left(\log\ Re\right)^{3/2}} \sim \frac{Ra^{1/2}}{\left(\log\ Ra\right)^{3/2}} \tag{2}$$

where $Re \sim Ra^{1/2}$ is Reynolds number of velocity fluctuations in the plates' vicinity [57]. A simple way to derive the asymptotic $Nu \sim Ra^{1/2}$ scaling of the numerator consists in a dimensional analysis which neglects the contribution of diffusive processes (viscous and thermal diffusivities) in the overall transport [65]. In practice, a viscous sub-layer always persists at the walls due to the non-slip condition at the fluid-solid interface. The log correction of the denominator of equation (2) arises from the Re dependence of the thickness of this viscous boundary sublayer. In a cell with a roughness matching the thickness of the thermal boundary layer at the transition, the sublayer thickness is no longer Re dependence, the log correction cancels and the pure $Nu \sim Ra^{1/2}$ scaling recovered, as predicted [66] and observed [67, 68].

Variants of Kraichnan's model, with different corrections from the pure $Nu \sim Ra^{1/2}$ scaling, have been proposed (see eg. [15, 28, 57, 69]) as well as a class of models based on extremum methods, that provides some bounds for heat transfer law in the fully turbulent case (see e.g. [70–73]). For alternative approaches of the flow regimes at very high Ra, see for example [61, 63].

1.4. Datasets reaching very high Ra

Table 1 summarizes the main specifications of the Rayleigh–Bénard experiments discussed in the present paper. For convenience, names picked from previous publications are given to experiments when their geographical location and aspect ratio are insufficient to identify them unambiguously (3rd column of the table). The table includes most experiments[5] reaching at least $Ra \simeq 10^{13}$. Data will be restricted within $0.6 \lesssim Pr \lesssim 7$ and some data considered as non-Boussinesq by their authors are discarded. The two cells with rough surfaces reaching very high Ra will not be further discussed [67, 68], but the interpretation presented in the original paper are consistent with the model proposed in this study[6].

---

[3] Bypassing the boundary layer resistance is possible thanks to a radiative heating or cooling of the bulk of the flow (eg see [125, 126]).
[4] Below the transition, the boundary layer is not laminar is a classical way. It is indeed fluctuating both in space and time (eg. [78, 127, 128]).
[5] The few very high Ra experiments performed in deliberately altered Rayleigh–Bénard cells are not listed here. For instance, some used screens inserted within the flow and others heaters/cooler attached to the sidewall [16].
[6] The heat transfer Nu(Ra) can be improved beyond a threshold Ra without occurrence of the ultimate state: this occurs for instance at low Ra in rough cells, when the boundary layer thickness reaches the typical height of the roughness (eg. see [129]) which leads to an increase of the effective surface contributing to heat transfer, and therefore on the effective surface contributing to heat transfer, different Nu(Ra) scalings can appear (eg. see [130]) and they should not be confused with a signature of the ultimate state. Only two studies have been performed with rough cells at high Ra, in conditions where a heat tranfer transition is also observed in the corresponding cell with smooth walls: both reported a Nu(Ra) scaling exponent close to 0.5, consistent with the present model ([67, 68]).

Some experiments in large water cells reach 'only' Ra $\simeq 10^{12}$ and they will not be discussed due to the limited range of very-high Rayleigh numbers. Indeed, only a few data with the largest Ra are likely to experience a heat transfer increase, but possible non-Boussinesq deviations make evidence less conclusive. Among these water experiments, two do not report a heat transfer enhancement (in Honk-Kong [74] and Lyon [75]) while one does (in Minneapolis [76]).

Direct numerical simulations (DNS) are not able yet to achieve high-enough Ra to observe a transition to the ultimate state, at least in 3D and arguably in 2D [12, 13]. Still extrapolation of the shear Re of the boundary layer at high Ra (eg. see [77, 78]) suggests that this transition is within reach of experiments (see also [57, 69]). Very large eddy simulations allowed to reach Rayleigh numbers up to Ra = 10^{15} and gave clear indication of a possible transition above Ra = 10^{13} [79].

2. A minimalist model accounting for all observations

We now make three simple conjectures about the transition to the ultimate state of convection, and show that they allow to account for most experimental observations.

2.1. Conjecture #1: a sub-critical transition to the ultimate state

The transition to turbulence of classical boundary layers has been a very rich and active field of investigation over more than 150 years [81] and the general properties of this transition have been well identified (e.g. see reviews [82–86]). In contrast, our understanding of transition in the boundary layers of Rayleigh–Bénard cells is still in its infancy. For example, there is no consensus on the scenario(s) which lead(s) to its destabilization, nor on the assessment of the shear stresses appearing in the boundary layers at given Ra and Pr.

The complexity of Rayleigh–Bénard boundary layers, compared to classical boundary layers, arises from a number of reasons including the close nature of the flow, the coexistence of energy transfer from small-to-large scales and vice-versa due to the build-up of a large scale wind associated with a collective motion of thermal plumes, the unsteady dynamics of the boundary layers even in their laminar state, feedback mechanisms between thermal and mechanical forcing, the interplay between viscous and thermal scales... In experimental and numerical set-ups, extra difficulties arise from the finite lateral extent of the convection cell, resulting in non-homogeneity in the horizontal direction. Given these peculiarities, the theory of classical boundary layer transition is not expected to provide accurate predictions in Rayleigh–Bénard cells. Still, by lack of well-accepted theoretical alternatives, the classical theory of turbulent boundary layer provides a customary framework for modeling turbulent boundary layer in convection cells. Along this line, our model is built from analogies and comparisons with robust qualitative features of classical transitions.

The transition of a classical boundary layers is most often described as a *globally sub-critical* process: in the transitional region, the flow is a mix of laminar and turbulent phases, separated by a sharp interface evolving *intermittently* in space and time. In this transitional region, the system response becomes very sensitive to flow details such as roughness, wall curvature, free-stream turbulence, sound, perturbations... a well-known property called 'boundary layer *receptivity*' [82, 87].
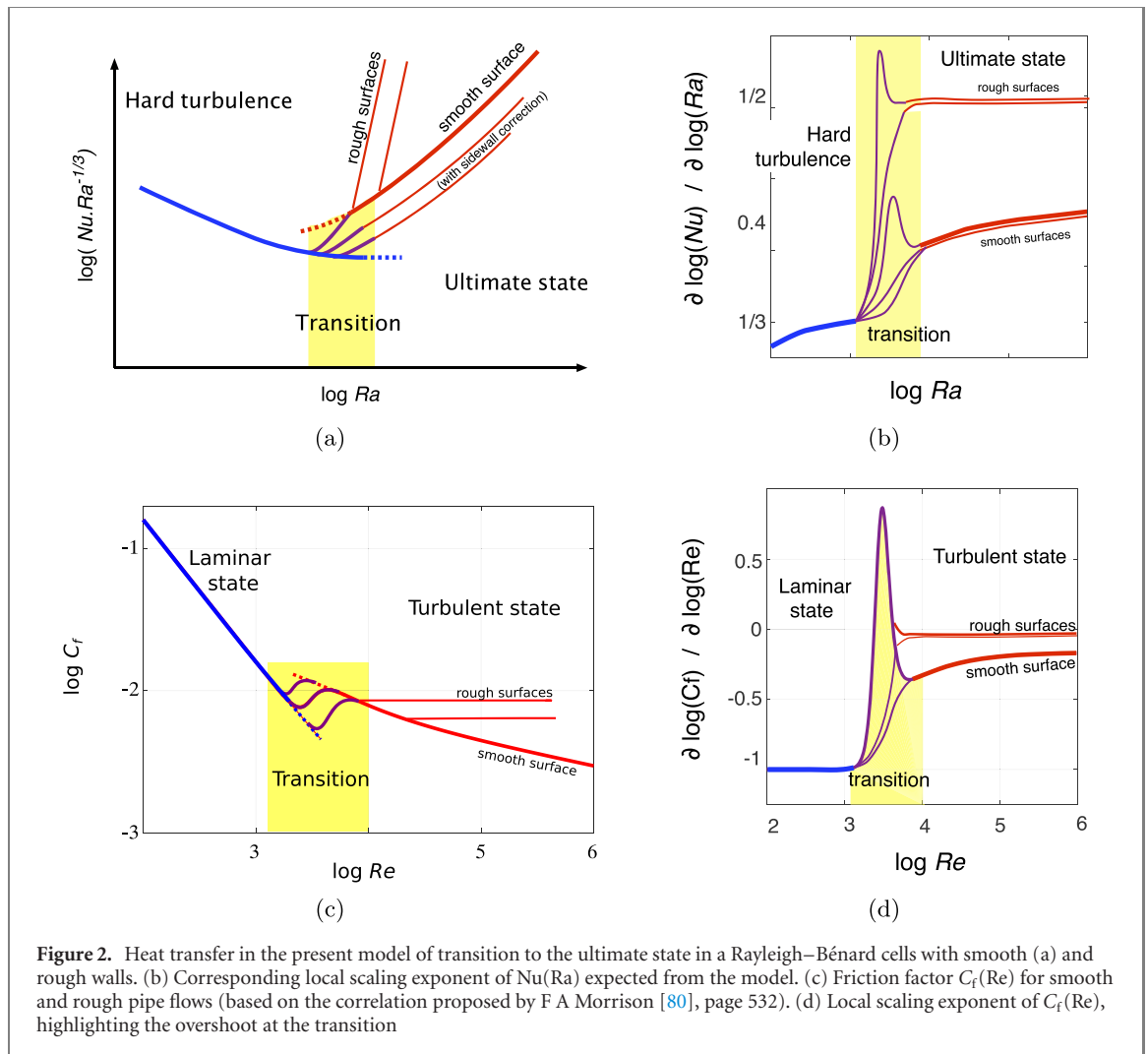
Our first conjecture is that the transition to the ultimate state in Rayleigh–Bénard cells of infinite aspect ratio is globally sub-critical.

In cells of finite aspect ratio Γ, confinement by the lateral sidewall alters the horizontal homogeneity of the boundary layers by direct mechanisms (eg momentum and heat exchanges) and indirect ones (eg. constrains on the large-scale flows and corner flows). This non-homogeneity of the boundary layers will inevitably produce some smoothing of the transition [78], and can contribute to restore some apparent continuity of the crossover between the hard turbulence state and the ultimate one.

The expected consequence of this first conjecture on the average heat transfer is summarized by the sketches of figures 2(a) and (b), which show respectively the compensated Nu(Ra) and local scaling exponent of Nu(Ra) in convection cells with smooth and rough walls.

An analogy between heat transfer in a convection cell and momentum transfer in a transiting pipe flow [86, 88] is interesting as both processes are controlled by a balance of diffusive or/and turbulent transport across boundary layers. This analogy is emphasized by the friction factor C_f(Re) plots of figures 2(c) and (d), which mirror the subplots a and b. The dimensionless friction factor C_f is defined as the normalized pressure drop δp per unit length along a pipe:

$$C_f(\text{Re}) = \frac{\delta p}{\delta p_{\text{turb}}}$$

Figure 2. Heat transfer in the present model of transition to the ultimate state in a Rayleigh–Bénard cells with smooth (a) and rough walls. (b) Corresponding local scaling exponent of Nu(Ra) expected from the model. (c) Friction factor C_f(Re) for smooth and rough pipe flows (based on the correlation proposed by F A Morrison [80], page 532). (d) Local scaling exponent of C_f(Re), highlighting the overshoot at the transition

where $\delta p_{\text{turb}} = \rho V^2 / 2D$ is proportional to the pressure drop that would appear along a pipe due to a purely turbulence drag (D, ρ and V are respectively the pipe diameter, the fluid density and the mean flow velocity)[7]. The absence of saturation of C_f(Re) at very large Re (see figure 2(c)) is well understood as the result of a log correction associated with the viscous sublayer at the (smooth) walls. As discussed earlier, the same type of correction is present in Kraichnan's model of the ultimate state, and it is depicted in subplot a and b.

One key feature of so-called *globally sub-critical transitions* is the existence of two distinct states, characterized here by their respective Nu(Ra) or C_f(Re) dependences, displayed in blue and red on figure 2. The bistable cross-over from one state to the other (yellow region) is expected to be *intermittent* and highly *receptive* to the details of its environment. Thus, over the transitional range, a non-universal cross-over Nu(Ra) is expected (purple curves). Contrariwise, the ultimate state is expected to have more universal properties, modulo sidewall corrections in small Γ cells.

We now explore if published data support this first conjecture. In particular we look if the transitions reported at high Ra in Rayleigh–Bénard cells present evidence of three key features of globally sub-critical transitions:

(a) A cross-over between two *distinct* states.

(b) *Receptivity* of the transition to tiny changes.

(c) *Intermittent* fluctuations in the transitional range.

---

[7] The Nusselt number is defined by normalizing heat transfer P by a purely diffusive (heat) transfer Pdif (see equation (1)) while the friction factor Cf normalization is done with a purely turbulent (momemtum) transfer. To make a more complete analogy, heat transfer P across a convection cell could be normalized by a purely turbulent heat transfer proportional to$P_{\text{turb}} = P_{\text{dif}} \cdot \sqrt{\text{Ra.\,Pr}}$. This expression for Pturb is derived from dimensional considerations imposing than Pturb should not depend on the viscous and thermal molecular diffusivities ν and κ of the fluid [65].
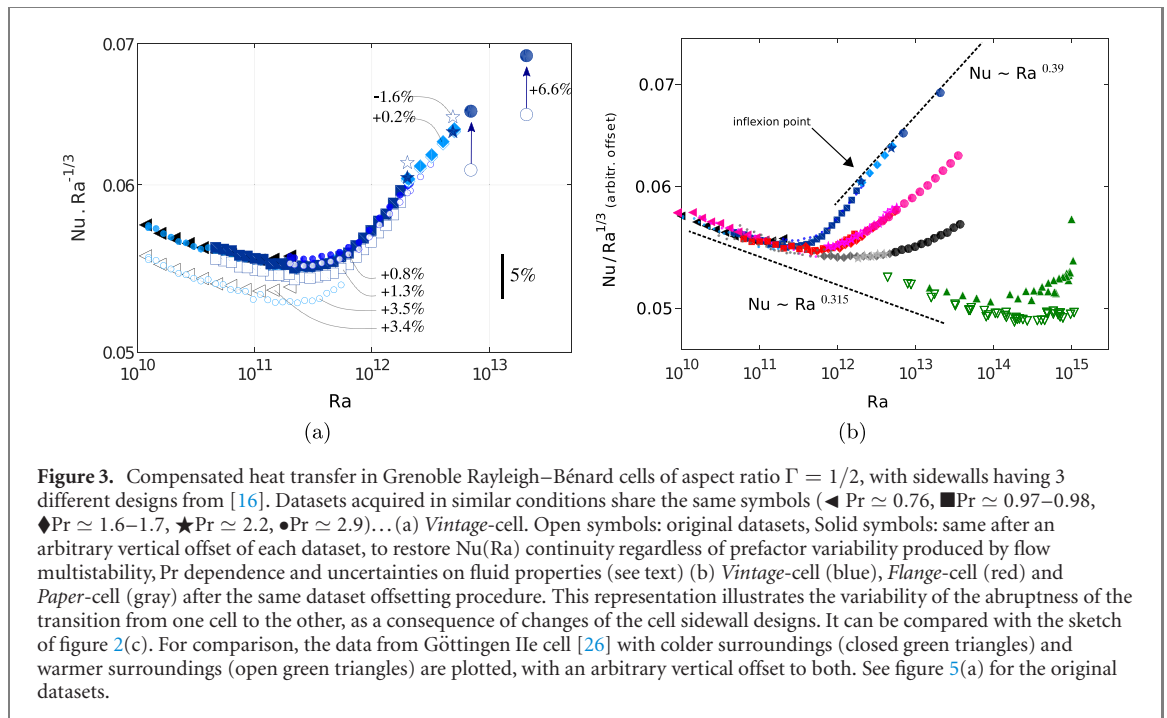
Figure 3. Compensated heat transfer in Grenoble Rayleigh–Bénard cells of aspect ratio $\Gamma = 1/2$, with sidewalls having 3 different designs from [16]. Datasets acquired in similar conditions share the same symbols (◀ $Pr \simeq 0.76$, ■$Pr \simeq 0.97-0.98$, ♦$Pr \simeq 1.6-1.7$, ★$Pr \simeq 2.2$, ●$Pr \simeq 2.9$)…(a) *Vintage*-cell. Open symbols: original datasets, Solid symbols: same after an arbitrary vertical offset of each dataset, to restore Nu(Ra) continuity regardless of prefactor variability produced by flow multistability, Pr dependence and uncertainties on fluid properties (see text) (b) *Vintage*-cell (blue), *Flange*-cell (red) and *Paper*-cell (gray) after the same dataset offsetting procedure. This representation illustrates the variability of the abruptness of the transition from one cell to the other, as a consequence of changes of the cell sidewall designs. It can be compared with the sketch of figure 2(c). For comparison, the data from Göttingen IIe cell [26] with colder surroundings (closed green triangles) and warmer surroundings (open green triangles) are plotted, with an arbitrary vertical offset to both. See figure 5(a) for the original datasets.

2.1.1. Evidence for two distinct states

Super-critical transitions are characterized by a continuous bifurcation between two states without transitional region. In contrast, *sub-critical* ones evidence a transitional region between two pure states, here the 'hard turbulence' and 'ultimate' states. Thus, the challenge is to find evidence of well defined markers for the onset and the end of a transitional region. This requires high resolution datasets.

For this purpose, rather than focusing on the Nu(Ra) dependence, it is more informative to focus on its local scaling exponents γ

$$\gamma(\mathrm{Ra}, \mathrm{Pr}) = \left(\frac{\partial \log \mathrm{Nu}}{\partial \log \mathrm{Ra}} \right)_{\mathrm{Pr}} \tag{3}$$
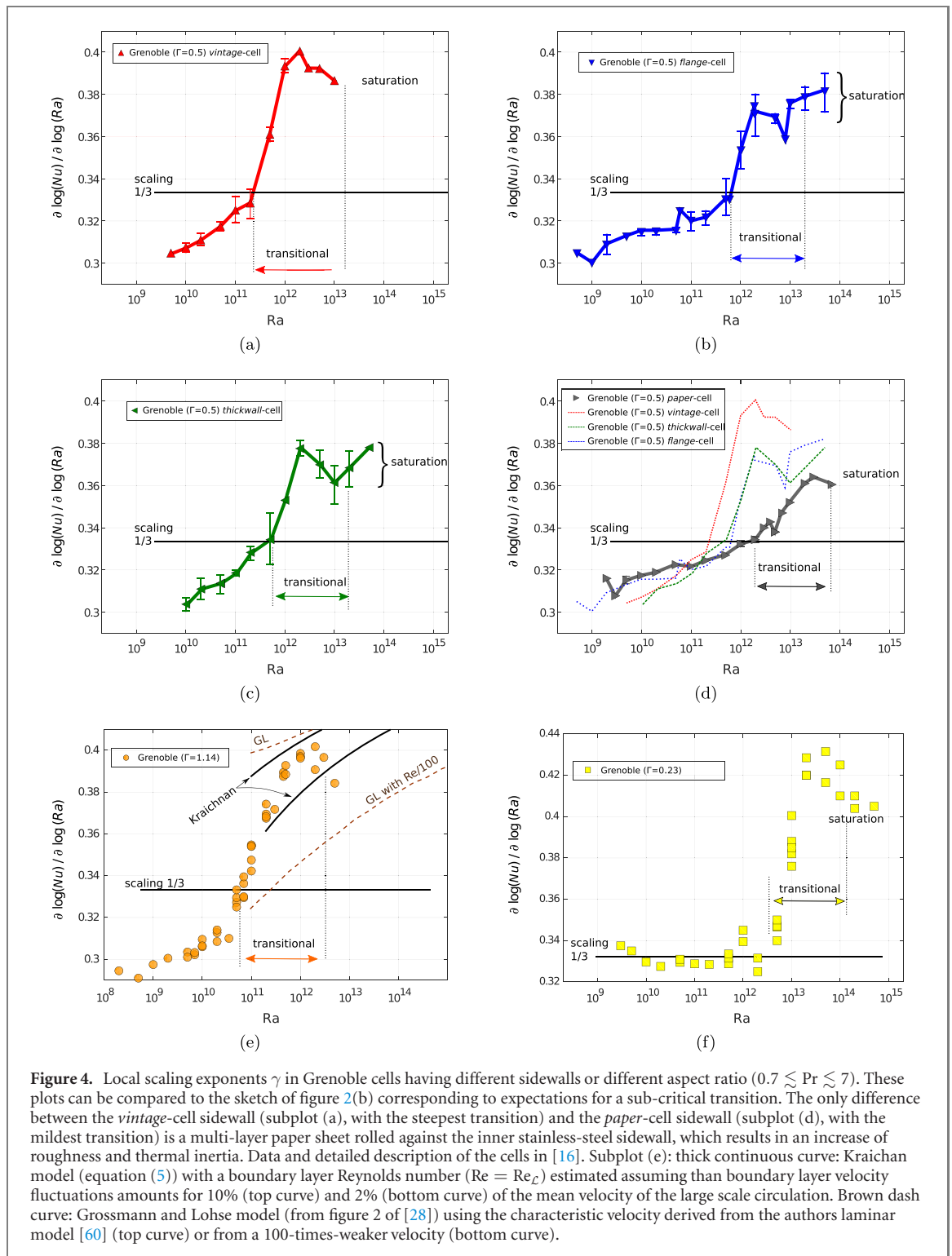
provided that it can be determined with sufficient accuracy. Indeed in specific experimental conditions (listed later), three sources of scatter of Ra and Nu data can be circumvented by focusing on local scaling exponents. These sources of scatter are the uncertainty on fluid properties, the Pr dependence and a statistical bias due to flow multi-stability. The last bias is caused by rearrangement of the large scale flow between quasi-stable configurations over long macroscopic diffusive time scales (of order a fraction of $h^2/\kappa \simeq h^2/\nu$) [45, 46, 52, 53, 75, 89, 90]. It has been reported that such changes of configurations essentially result in heat transfer offsets, up to 7% percents in $\Gamma = 1/2$ cell [54] and 14% for $\Gamma = 0.23$ [16]. Fortunately, in specific conditions, these 3 sources of scatter are only responsible for nearly constant prefactor corrections on Nu, so they nearly leave unchanged the local scaling exponent γ of Nu(Ra), at least over a limited range of Pr.

The specific conditions to benefit from constant prefactor offsets between datasets can often be met by performing a sequential acquisition faster than the macroscopic diffusive time (to reduce the chances of large-scale-flow rearrangement), at a fixed mean temperature and density, thus at constant Pr and fluid properties. A consistency check of the constancy of prefactors is done *a posteriori* on a log-log plot of Nu(Ra): datasets obtained in different conditions should collapse thanks to a small vertical offsetting, as illustrated on figures 3(a) and (b) in the restricted range $0.7 < \mathrm{Pr} < 3$.

Different mean flow configurations could exhibit different scaling exponents, or the apparent exponent could be biais by a continuous drift in the flow rearrangement. We never experienced such conditions but their existence cannot be excluded, and such conditions would reduce the benefit of this method. That is why the consistency check mentioned above should be performed.

Another advantage to focus on the scaling exponent $\gamma(\mathrm{Ra})$ rather than Nu(Ra) is the possibility of direct comparison with the predictions of convection models, which rarely provide precise numerical prefactors.

The plots of figure 4 present exponents $\gamma(\mathrm{Ra})$ measured in Grenoble cells with different sidewall properties, all within $0.7 \lesssim \mathrm{Pr} \lesssim 7$. All the data are from [16]. The exponents at Ra_0 were determined by plotting $\mathrm{Nu.Ra}^\sigma$ versus Ra and adjusting manually the compensation exponent σ till the operator deemed the curve horizontal at Ra_0. The errorbars on the exponents correspond to the margin of error on σ

Figure 4. Local scaling exponents γ in Grenoble cells having different sidewalls or different aspect ratio ($0.7 \lesssim \Pr \lesssim 7$). These plots can be compared to the sketch of figure 2(b) corresponding to expectations for a sub-critical transition. The only difference between the *vintage*-cell sidewall (subplot (a), with the steepest transition) and the *paper*-cell sidewall (subplot (d), with the mildest transition) is a multi-layer paper sheet rolled against the inner stainless-steel sidewall, which results in an increase of roughness and thermal inertia. Data and detailed description of the cells in [16]. Subplot (e): thick continuous curve: Kraichan model (equation (5)) with a boundary layer Reynolds number (Re = Re$_{\mathcal{L}}$) estimated assuming than boundary layer velocity fluctuations amounts for 10% (top curve) and 2% (bottom curve) of the mean velocity of the large scale circulation. Brown dash curve: Grossmann and Lohse model (from figure 2 of [28]) using the characteristic velocity derived from the authors laminar model [60] (top curve) or from a 100-times-weaker velocity (bottom curve).

assessed by the operator. The procedure was performed independently by two operators (first and second authors of [16]) and led to very similar results (the worst errorbar was retained).

One remarkable feature is the common general shape of all γ (Ra) dependences, with a break when $\gamma(\mathrm{Ra}) \simeq \frac{1}{3}$ (or slightly earlier for the $\Gamma = 1.14$ cell) interpreted as the onset of the transitional region, and with a saturation of the exponents within $\gamma \simeq 0.36$–0.40, interpreted as the end of the transitional region. The saturation exponents cannot be accurately determined because the plateau regions are only reached by a few points. Nevertheless, the non-monotonic variations of the exponent versus Ra and the leveling of exponents around 0.38 ± 0.02 (at the highest Ra) are robustly observed in the 6 experiments. Two qualitative markers can thus be clearly identified. The overshoot observed before saturation of γ (Ra) in the Grenoble-vintage cell corresponds to the inflection point visible on figure 3(b) and is reminiscent of the inflection point of friction factor C_f(Re) for pipe flows at the transition, as illustrated by figures 2(c) and
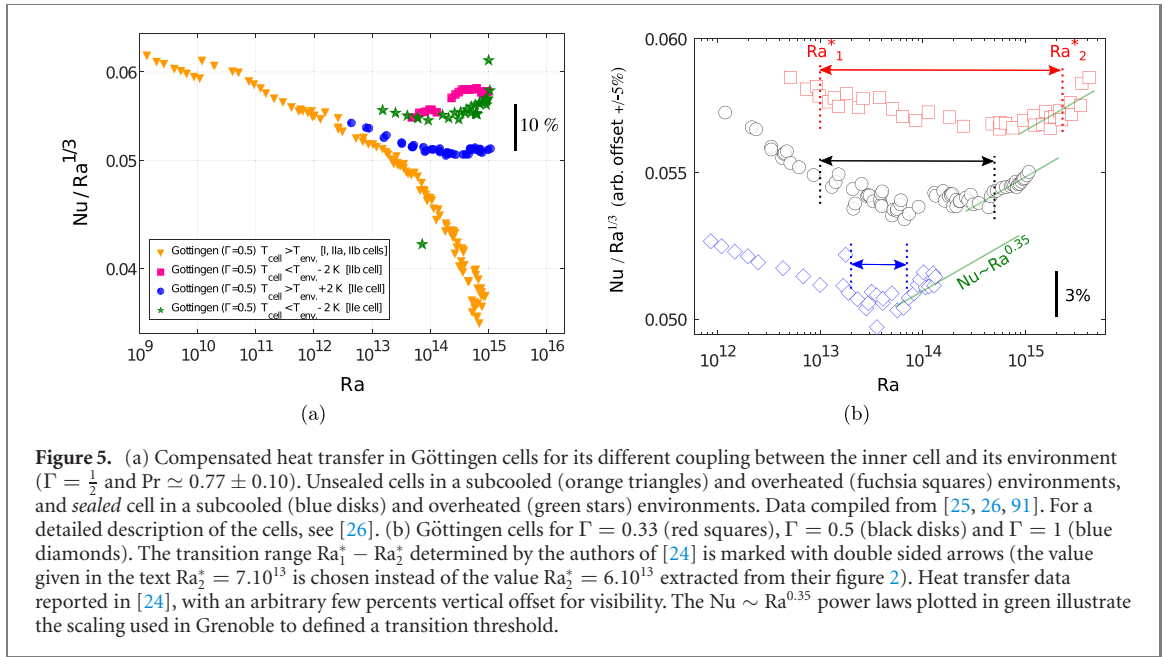
Figure 5. (a) Compensated heat transfer in Göttingen cells for its different coupling between the inner cell and its environment ($\Gamma = \frac{1}{2}$ and Pr $\simeq 0.77 \pm 0.10$). Unsealed cells in a subcooled (orange triangles) and overheated (fuchsia squares) environments, and *sealed* cell in a subcooled (blue disks) and overheated (green stars) environments. Data compiled from [25, 26, 91]. For a detailed description of the cells, see [26]. (b) Göttingen cells for $\Gamma = 0.33$ (red squares), $\Gamma = 0.5$ (black disks) and $\Gamma = 1$ (blue diamonds). The transition range $Ra_1^* - Ra_2^*$ determined by the authors of [24] is marked with double sided arrows (the value given in the text $Ra_2^* = 7.10^{13}$ is chosen instead of the value $Ra_2^* = 6.10^{13}$ extracted from their figure 2). Heat transfer data reported in [24], with an arbitrary few percents vertical offset for visibility. The Nu $\sim Ra^{0.35}$ power laws plotted in green illustrate the scaling used in Grenoble to defined a transition threshold.

(d). The existence of an overshoot followed by a saturation of $\gamma(Ra)$ is one of the strongest evidence of the existence of separated Nu(Ra) branches for the hard turbulence and ultimate states. These observations support the transition pictured by figure 2(a), of a transitional region between two pure states. The precise extension of the transitional range is delicate to assess precisely by lack of data at large enough Ra (see double sides arrows) but an estimate is 1.5 decade of Ra.

2.1.2. Evidence of boundary layer 'receptivity'
We now need to verify if the transition observed at very high Ra is very sensitive to small change of the set-up, as expected for sub-critical transition of boundary layers.

Receptivity to the sidewall properties. Figure 4.d gathers on a single plot the γ (Ra) dependences observed in four Rayleigh–Bénard cells operated in similar experimental conditions, with the same top and bottom plates but which differ by the thickness and material of their sidewalls. The cell with the thinnest stainless steel sidewall (Grenoble-*vintage* cell) has the most abrupt transition, in particular compared to the *thickwall*-cell with its 4.4-times-thicker walls. The mildest Nu(Ra) increase is found in the Grenoble-*paper* cell, where the thin stainless steel sidewall is thermally isolated from the convecting fluid by a quiescent layer of fluid trapped in the pores of a multilayer paper roll (see table 1 for details). Interestingly, the Nu(Ra) increase in this cell is as mild as the one reported in Göttingen, as can be see on figure 3(b). Thus, the transition is found to be highly sensitive to small changes in the sidewall construction, which can be seen as a first evidence of boundary receptivity.

Receptivity to heat and mass exchange between the cell and its environment. The Göttingen cell is not perfectly isolated from its surrounding and successive modifications, as well as tests in various thermal configurations, have produced differences in Nu(Ra). Figure 5(a) encompasses heat transfer measurements for $\Gamma = 0.5$, as reported in three papers [25, 26, 91]. The triangles and square symbols correspond to 'unsealed' cells (*cells* I, IIa and IIb), allowing mass exchange through gaps along the sidewall between the cell and its surrounding environment, while a filling valve has been added to fill/empty the cell IIe used for the two other datasets (disks and stars). The two upper sets of data (squares and stars) have been obtained with a mean cell temperature colder by at least 2 K than its surrounding, while the two lower datasets with a cell hotter than its environment. Interestingly, both mass and thermal exchanges with the environment result in a heat transfer change exceeding 10%, that is larger than the increase of Nu attributed to the transition to the ultimate regime in these cells. It is difficult to speculate on the various physical mechanisms which produce such significant variations of heat transfer from one cell to the other, in particular when the apparent Nu(Ra) scaling becomes lower than in the regime at lower Ra. Still, these datasets suggest that the heat transfer, and therefore the boundary layer which controls it, becomes very sensitive to perturbations coming from the cell environment.

Receptivity to change of aspect-ratio Γ. It is delicate to define precisely the Ra numbers for the onset and end of the transitional region. Indeed, most definitions tend to depend on models or expectations of the flows before and after the transition, and there is consensus on neither one. In Grenoble, conservatively, a unique characteristic transition Ra_U was defined [16]: it corresponds to the Rayleigh number for which

$\gamma(\mathrm{Ra})$ reaches the arbitrary threshold exponent $\gamma(\mathrm{Ra_U}) = 0.35$. This threshold exponent is chosen to be intermediate between the largest exponent predicted for hard turbulence state ($\gamma = \frac{1}{3}$) and the lowest exponent at which $\gamma(\mathrm{Ra})$ saturates at very high Ra, after the transition. An aspect ratio dependence $\mathrm{Ra_U} \sim \Gamma^{-2.5\pm0.5}$ was reported within $0.23 \leqslant \Gamma \leqslant 1.14$ [16]. It is clear from figures 5 and 12(a) from [16], as well as present figure 4 that the onset and end of the transitional region have a nearby Γ dependence. The Göttingen and Santa-Barbara groups interpret their measurements using the Grossman–Lohse model, and reciprocally their experimental data play a key role in the developments and parameters fitting of this model (eg. see [28, 92]). This synergy allows the former to determine lower and upper bounds $\mathrm{Ra_1^*}$ and $\mathrm{Ra_2^*}$ for transitional range, based on expectations of the scalings before the transition (they expect it to be significantly lower than Malkus' $\frac{1}{3}$) and after the transition (expected to be 0.38, without overshoot of $\gamma(\mathrm{Ra})$). For reference, an alternative interpretation of same measurements based on Malkus scaling, rather than Grossman–Lohse's, is proposed in [14]. Figure 5(b) shows the determined bounds $\mathrm{Ra_1^*}$ and $\mathrm{Ra_2^*}$ for $\Gamma \in \{0.33, 0.5, 1\}$. The authors found a weak dependence for $\mathrm{Ra_1^*}(\Gamma)$ [27], but a significant one for $\mathrm{Ra_2^*}(\Gamma)$, with a $\mathrm{Ra_2^*} \sim \Gamma^{-3.26}$ scaling [24]. For comparison, the figure also shows in green the $\mathrm{Nu} \sim \mathrm{Ra}^{0.35}$ scaling used in Grenoble to define the transition threshold $\mathrm{Ra_U}$. Within accuracy, this threshold definition would have lead to $\mathrm{Ra_U} \simeq \mathrm{Ra_2^*}$. Strikingly, both scalings of $\mathrm{Ra_U}(\Gamma)$ and $\mathrm{Ra_2^*}(\Gamma)$ are compatible suggesting a common underlying physics in Grenoble and Göttingen. The difference of the prefactors of both scaling laws is addressed later.

In all cases, the present observations are a third set of evidence that the transition is highly sensitive to the details of the cell, here lateral confinement by the sidewall. Later in this paper, we propose a quantitative physical interpretation for this aspect ratio dependence.

To summarize, we have three independent sets of evidence of the great *receptivity* of transition thanks to:

- Change of sidewall material and geometry, systematically tested in Grenoble.
- Change of parasitic heat and mass exchanges with the surrounding of the cell, reported in Göttingen.
- Change of the cell aspect ratio, with consistent scalings of the transitional Ra in Grenoble and Göttingen.

For reference, we recall that three systematic changes of plate properties had little influence of the transition: plate material modified from copper to brass [68], plate with an uneven surface [93] and plate unpolished by sand-blasting (unpublished).

2.1.3. Evidence of intermittent fluctuations

Sub-critical transitions exhibit so-called *intermittent* fluctuations in the transitional region, due to the spatio-temporal competition between the laminar and turbulent states. These fluctuations have been reported in the literature even before Reynolds seminal article on pipe flow transitions [94]. The continuity of the friction factor $C_f(\mathrm{Re})$ in the transitional range of pipe flows reflects the mean properties of these underlying macroscopic fluctuations (e.g. see [95]). By analogy, we need to verify if similar intermittent fluctuations are present in Rayleigh–Bénard cells concomitantly with the heat transfer enhancement attributed to the ultimate regime. We review below the existing measurements of local and integral fluctuations at the transition[8].

Local temperature fluctuations. Non-invasive measurements within the boundary layers are very delicate due to its small thickness (typically $\lambda = h/2.\mathrm{Nu} \simeq 0.2$ mm at the transition in Grenoble 20 cm-high cells and Göttingen 224 cm-high cell). A direct test of the flow state of the boundary layer is therefore difficult. Nevertheless, a probe can be positioned right above the boundary layer. In Grenoble, such a probe sees extra fluctuations at the transition, with a change of second order statistics, as reported in [15] and later confirmed independently [96] with a probe 10 ten times smaller, having a sensitive spot of size 17 μm.

The Göttingen group has also reported local temperature measurements above the bottom boundary layer. In contrast with Grenoble, no signature of a transition was found and it concludes that the spectral shape of temperature fluctuations is *universal* [97], in other words that the transition to turbulence of thermal boundary layers does not lead to any change in the second order statistics of the temperature above the boundary layer. This surprising observation may result from the positioning the sensor close to the sidewall, contrary to the positioning chosen in Grenoble near the plates axis. The stronger large-scale wind present in Gottingen cell at high Ra (later discussed) may also contribute to hide a transition of the thermal boundary layer.

---

[8] In the context of Rayleigh–Bénard convection over rough plates, not discussed in the present paper, intermittent bursts of coherent plumes have been reported, as well as increase of heat transfer and root-mean-square (rms) fluctuations of the velocity above a transition threshold associated with roughness height [75]. As suggested by J Salort (private communication), the present interpretation framework may be relevant in this case too.
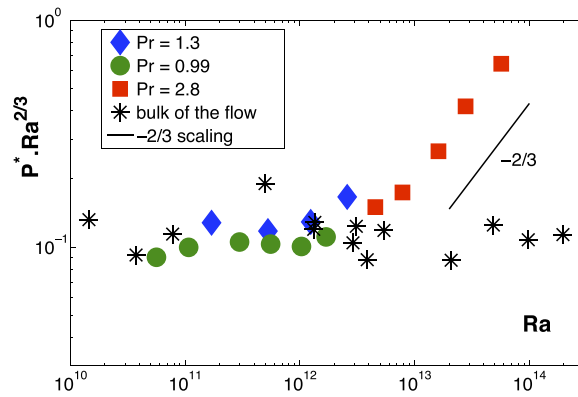
Figure 6. Compensated spectral density P^* of the slow temperature fluctuations of the bottom plate (full symbols) and corresponding quantity in the bulk of the flow (stars) in a cell of aspect ratio $\Gamma = \frac{1}{2}$. The increased fluctuations observed for $Ra \gtrsim 3 \times 10^{12}$ in the bottom plates -compared to the core of the flow- evidence the emergence of fluctuations of thermal resistance across the bottom boundary layer. Data from [98].

Integral fluctuations of the heat transfer. Taking advantage of the very large thermal diffusivity of copper at low temperature, which is nearly 4 decades larger at 6 K than at 300 K, the spatially-averaged fluctuations of the heat leaving the bottom plate are proportional to fluctuations the plate temperature, which can be resolved [98]. The spectra of the integral fluctuations of heat flux (in practice the bottom plate temperature) exhibit a low frequency plateau followed by a cut-off. As customary in shot noise characterization, e.g. in photonic and electronic transport, the power spectral density level of the low frequency the plateau can be used to characterize the integral fluctuations. In practice, this density (in $K^2\ Hz^{-1}$) is normalized by $\Delta^2 h^2/\nu$ to become a dimensionless quantity labelled P^* in figure 6 [98]. The Grenoble group emphasized that their observed Nu(Ra) transition is concomitant with the emergence of strong fluctuations of the heat flux across the bottom boundary layer, as illustrated by figure 6. Besides, these emerging fluctuations are highly non-gaussian [98]. If they were produced from a large number of degrees of freedom (e.g. numerous unstable plumes), the central limit theorem would have gaussianized them. In contrast, non-gaussianity is consistent with the picture of a few competing laminar and turbulent regions, each having a significant contribution to the total heat transfer. This picture is highly reminiscent of the intermittent fluctuations associated with transition of classical boundary layers (eg. see [99]). Still, one cannot reject the original interpretation proposed in [98] which attributes the increase of fluctuations to intrinsic turbulent dynamics of the boundary layer in the ultimate state, rather than attributing them to the intermittent switching between the hard turbulence state and the ultimate state.

To summarize, we listed indirect evidences of the intermittent fluctuations of the boundary layer at the transition, both from local and integral measurements conducted in Grenoble. In contrast, local temperature measurements close to the plate-sidewall corner of Göttingen cell did not evidence any statistical signature of a transition.

2.2. Conjecture #2: macroscopic boundary layer eddies control the transition

Classical turbulent boundary layers are often described, using a similarity-assumption, as a continuous superposition of eddies of sizes z positioned at a distance z from the wall. At first approximation, this phenomenological picture is successful in accounting for the famous log law-of-the-wall of the velocity profile and for the constant momentum flux across the boundary layer [100]. In the ultimate state, following Kraichnan's original model, we thus expect that a similar superposition of eddies prevails to sustain a turbulent mean heat transfer away from the plates in the vertical direction. The conjecture below is based on this simple analogy.

In Rayleigh–Bénard cells, a dynamical network of line-shape plumes forms on both plates. At the bottom plate for instance, plumes rise, accelerate, swirl and cluster, while colder fluid flows toward the plate (when $\alpha > 0$) balancing mass fluxes (eg see [79, 101−106]). This results in unsteady swirls or coherent vortical structures of different sizes and finite lifetime above the plates [107−109]. The largest of these freely evolving structures will be named *boundary layer eddies*, or in short *bl-eddies*. As illustrated symbolically in two-dimensions (2D) by figure 7, we expect that the size $\mathcal{L}$ of bl-eddies to be either constrained laterally by the vertical sidewall in narrow cells (say $\Gamma \lesssim 2$) or vertically by the opposite horizontal plate in wide cells ($\Gamma \gtrsim 2$), resulting in a Γ-dependent characteristic length scale of order $\mathcal{O}\left(\min(h/2, \Phi/4)\right)$. For convenience, we define $\mathcal{L}$ as:
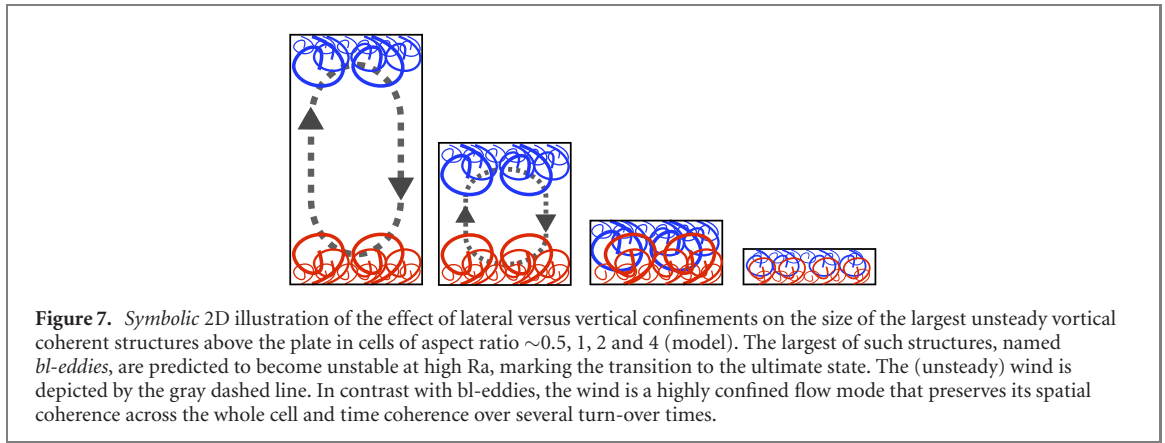
Figure 7. *Symbolic* 2D illustration of the effect of lateral versus vertical confinements on the size of the largest unsteady vortical coherent structures above the plate in cells of aspect ratio ∼0.5, 1, 2 and 4 (model). The largest of such structures, named *bl-eddies*, are predicted to become unstable at high Ra, marking the transition to the ultimate state. The (unsteady) wind is depicted by the gray dashed line. In contrast with bl-eddies, the wind is a highly confined flow mode that preserves its spatial coherence across the whole cell and time coherence over several turn-over times.

$$\mathcal{L} = \min\left(\frac{h}{2}, \frac{\Phi}{4}\right). \tag{4}$$

Our second conjecture states that these bl-eddies play a key role in the transition to the ultimate regime, the transition onset being associated to an instability determined by the characteristic Reynolds number $\mathrm{Re}_{\mathcal{L}}$ of these structures.

We now explore if published data support this second conjecture, in particular:

(a) An instability of bl-eddies occurring at the observed critical Rayleigh number.

(b) A transition controlled by the characteristic length scale $\mathcal{L}$ defined above.

2.2.1. Instability of bl-eddies at the transition

We need to check if the transitional Ra is consistent with an instability of bl-eddies. For that purpose, we need to estimate their typical $\mathrm{Re}_{\mathcal{L}}$ when the heat transfer transition is observed.

In cells of aspect ratio Γ of order unity, a large scale circulation *wind* (with characteristic Reynolds number $\mathrm{Re}_{\mathrm{wind}} \simeq V \cdot h/\nu$) fills the entire volume of the cell. This wind sweeps the rising (resp. falling) hot (resp. cold) plumes and benefit from their buoyancy to sustain its prominence over the velocity field inside the cell [77, 89, 90, 110, 111]. The wind strength has been extensively studied at very large Ra (eg [15, 16, 112, 113]) and was found to be hardly altered by the transition.

Thus, the mean wind velocity V is a first gross overestimate of the characteristic velocity of bl-eddies. A tighter overestimate is obtained from the characteristic velocity fluctuations of the wind over the boundary layers. The root-mean-square fluctuations of the wind velocity are known to amount for few tens of percents of its mean value (we arbitrarily take 25% below) [77, 89, 90, 110, 111]. Thus, for $\Gamma \simeq 1$ and $\mathrm{Ra} = 10^{11}$, a bl-eddy of size $\mathcal{L} = \Phi/4$ will have a typical Reynolds number of

$$\mathrm{Re}_{\mathcal{L}} = \frac{\mathcal{L} \cdot V_{\mathcal{L}}}{\nu} \lesssim \frac{(\Phi/4) \times (V.25\%)}{\nu} = \frac{\mathrm{Re}_{\mathrm{wind}}}{4} \times 25\%$$

and using the order of magnitude estimate $\mathrm{Re}_{\mathrm{wind}} \simeq \sqrt{\mathrm{Ra}}/10$, and taking $\mathrm{Ra} = 10^{11}$, we find

$$\mathrm{Re}_{\mathcal{L}} \lesssim \sqrt{\mathrm{Ra}}/160 \simeq 2000.$$

Typical transitional Reynolds number of classical shear flows [114] are in the few hundreds range[9]. The above overestimate of $\mathrm{Re}_{\mathcal{L}}$ is therefore compatible with the occurrence of transitions in Grenoble and Trieste cells at Ra where a heat transfer enhancement is reported[10].

A priori, one could argue that it is difficult to discriminate in practice between the above interpretation and the most common alternative interpretation, namely that the transition is directly triggered by the shear produced by the large scale circulation wind on the plates[11]. In fact, discriminating between both interpretations is possible because $\mathrm{Re}_{\mathcal{L}}$ and $\mathrm{Re}_{\mathrm{wind}}$ are predicted to be associated with different physical processes that can be varied independently. In particular, three experimental tests undertaken in Grenoble

---

[9] Plane Couette flows evidence transient turbulent spots above $\mathrm{Re} \simeq 280$, are unconditionally stable below $\mathrm{Re} \simeq 325$ and exhibit featureless turbulence above $\mathrm{Re} \simeq 415$ [85]. The same order of magnitude are found in other shear flows such as Taylor−Couette, torsional Coutte et plane Poiseuille channel flow [114].

[10] To our knowledge, no measurement below $\mathrm{Ra} = 4.10^{11}$ has been reported from Gottingen's $\Gamma \simeq 1$ cell. It would be interesting to perform very high resolution measurement in this range to examine the possibility of a hindered transition.

[11] This wind-shear interpretation, first proposed by Chavanne and collaborators [4], is a cornerstone of the model/experiment ecosystem elaborated by G Ahlers, E Bodenschatz, D Lohse and collaborators (eg. [26, 28]).

have evidenced a robustness of the transition Ra_U against modifications of Re_{wind}. Independent modifications of Re_{wind} were produced (1) by cell tilting, (2) by Pr variations[12] and (3) by insertion of 4 clogging screens in the flow at a distance $\geqslant 2\mathcal{L}$ from the plates [16]. These experimental observations seem hardly consistent with a transition instability triggered by a wind-shear in Grenoble. Besides this wind-shear scenario cannot explained the diversity of experimental results reported by various groups. The convergence of experimental findings against this pure wind-shear model of the transition has motivated the development of this second conjecture.

Quantitative consistency between this interpretation and Kraichnan's original prediction can be examined, while being mindful of Kraichnan warnings that his model is not expected to be accurate right above the transition. From equation (2) and (3), the scaling exponent γ predicted by Kraichnan is found to be

$$\gamma = 0.5 - \frac{3}{4 \ln Re},\tag{5}$$

(we took $Re \sim Ra^{1/2}$). Kraichnan's defines Re from the rms velocity at mid-height and from the characteristic length scale $h/2$. His definition matches the definition of $Re_\mathcal{L}$ in large aspect ratio cells (finite-Γ are not considered by Kraichnan), and leads to $\gamma = 0.4$ for $Re_\mathcal{L} \simeq 1800$ and $\gamma = 0.38$ for $Re_\mathcal{L} \simeq 500$. The quantitative agreement with the previous estimates and the measured exponents are found to be good.

Figure 4(e) displays the exponents estimated with Kraichnan model (equation (5)) generalized to finite Γ taking $Re = Re_\mathcal{L}$, and assuming that the typical velocity of bl-eddy amounts respectively for 10% and 2% of the typical velocity of the wind. We recall that Kraichnan model is not expected to be accurate right above the transition, according to its author. Predictions of the Grossmann and Lohse model [28] are also displayed for reference.

In the next section (conjecture #3), we will examine how a strong enough wind can alter *adversely* the bl-eddies instability, and explain the absence or limited heat transfer enhancements reported in some cells.

2.2.2. Evidence of a characteristic length scale $\mathcal{L}$ controlling the transition
Assuming for now that the wind does not alter significantly the strength of the bl-eddies, $Re_\mathcal{L}$ is expected to only depend on the macroscopic length scale $\mathcal{L}$, which implies on dimensional grounds

$$Re_\mathcal{L} \sim \mathcal{F}\left(Ra \cdot \frac{\mathcal{L}^3}{h^3}, Pr\right)$$

where $\mathcal{F}$ is an unknown function[13]. Assuming that the transition to the ultimate regime occurs when $Re_\mathcal{L}$ reached a critical Reynolds number, and using equation (4), we immediately see that the corresponding prediction for the transitional Rayleigh number $Ra_\mathcal{L}(\Gamma)$ scales as:

$$Ra_\mathcal{L} \sim \left(\frac{h}{\mathcal{L}}\right)^3 \sim \max\left(1, \frac{2^3}{\Gamma^3}\right).\tag{6}$$

As mentioned earlier, the transition Rayleigh number is observed to scale roughly like $\sim \Gamma^{-3}$ both in Grenoble [16] and Göttingen [24] within $0.23 \leqslant \Gamma \leqslant 1.14$. This is consistent with the prediction above. This scaling in mind, it is interesting to return to the Eugene/Trieste cells of aspect ratio $\Gamma = 0.5$, 1 and 4 to see if a similar Γ dependence can be discerned, although no evidence of transition was claimed by the authors of these studies. A close look at heat transfer data of figure 8(a) allows to single out two transitional Ra arbitrarily defined (for convenience) from the minimum value of $Nu.Ra^{-1/3}$ versus Ra for $\Gamma = 1$ and 4, and to define a third one based on the increase of data scatter above $Ra \simeq 10^{12}$ in the $\Gamma = 0.5$ cell. All the threshold Rayleigh numbers from Grenoble (Ra_U), Göttingen (Ra_2^*) and Eugene/Trieste are gathered in figure 8(b) with an arbitrary vertical offset applied to each subgroup of data. This important plot carries two (new) pieces of information.

First, a $Ra_\mathcal{L} \sim \Gamma^{-3}$ scaling still holds for $0.23 \lesssim \Gamma \lesssim 1.14$, which suggests that the increase of scatter in the $\Gamma = 0.5$ Eugene dataset can be interpreted as the signature of a damped, hindered or frustrated transition. By analogy, the significant increase of scatter observed in the Chicago data for $Ra \simeq 2 \times 10^{12}$ (see

---

[12] The wind strength Re_{wind} was varied at constant Ra taking advantage of its $\sim Pr - 0.75$ dependence.
[13] $\mathcal{F}$ is expected to have a weak Pr dependence within $1 \leqslant Pr \leqslant 3$ to account for experiments (see figure 7(a) of [16]) and a power law dependence of exponent $\simeq 0.4$–0.5 versus $\alpha.\Delta.g$, and therefore versus $Ra \cdot \frac{\mathcal{L}^3}{h^3}$, as most Reynolds numbers in turbulent Rayleigh–Bénard convection. The 'free-fall model' provides a justification of this dependence. A plume with zero initial velocity and experiencing a constant buoyant acceleration of $g.\alpha.\Delta/2$ will reach at a distance $\mathcal{L}/2$ from the plate the velocity $(\mathcal{L}.g.\alpha.\Delta/2)^{1/2}$, leading to the scaling law $Re_\mathcal{L} \sim Ra^{1/2}\left(\frac{\mathcal{L}}{h}\right)^{3/2}$. The Pr dependence has been omitted: it is probably not reliable in this free-fall model which ignores the diffusive processes such as those at play in plumes interaction. Corrections associated with the material properties of the sidewall are omitted here.
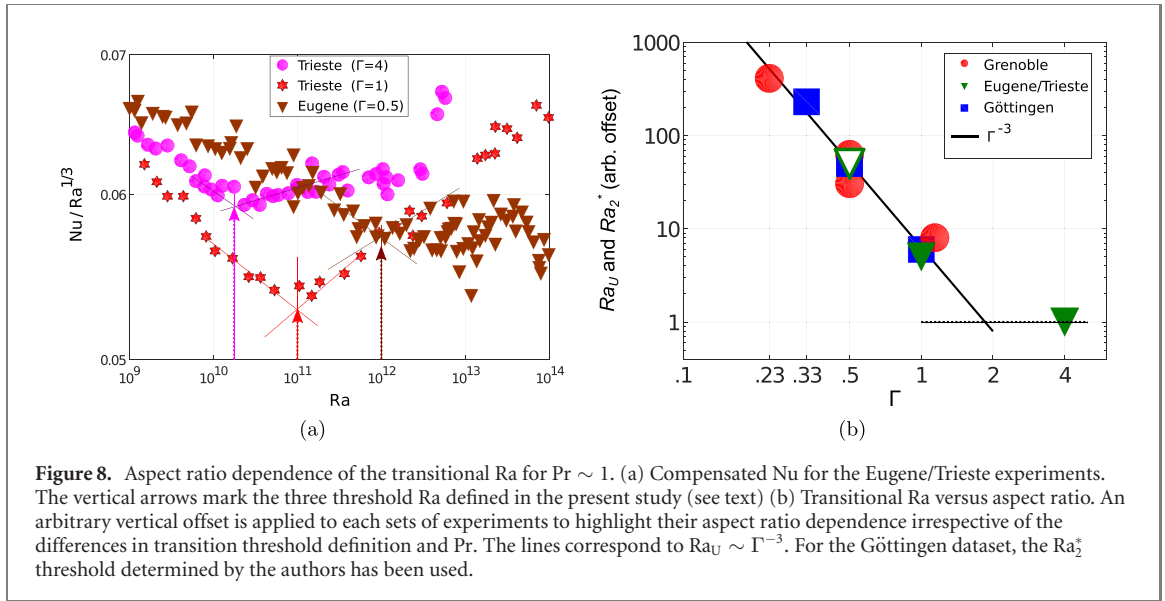
Figure 8. Aspect ratio dependence of the transitional Ra for Pr $\sim$ 1. (a) Compensated Nu for the Eugene/Trieste experiments. The vertical arrows mark the three threshold Ra defined in the present study (see text) (b) Transitional Ra versus aspect ratio. An arbitrary vertical offset is applied to each sets of experiments to highlight their aspect ratio dependence irrespective of the differences in transition threshold definition and Pr. The lines correspond to $Ra_U \sim \Gamma^{-3}$. For the Göttingen dataset, the Ra_2^* threshold determined by the authors has been used.
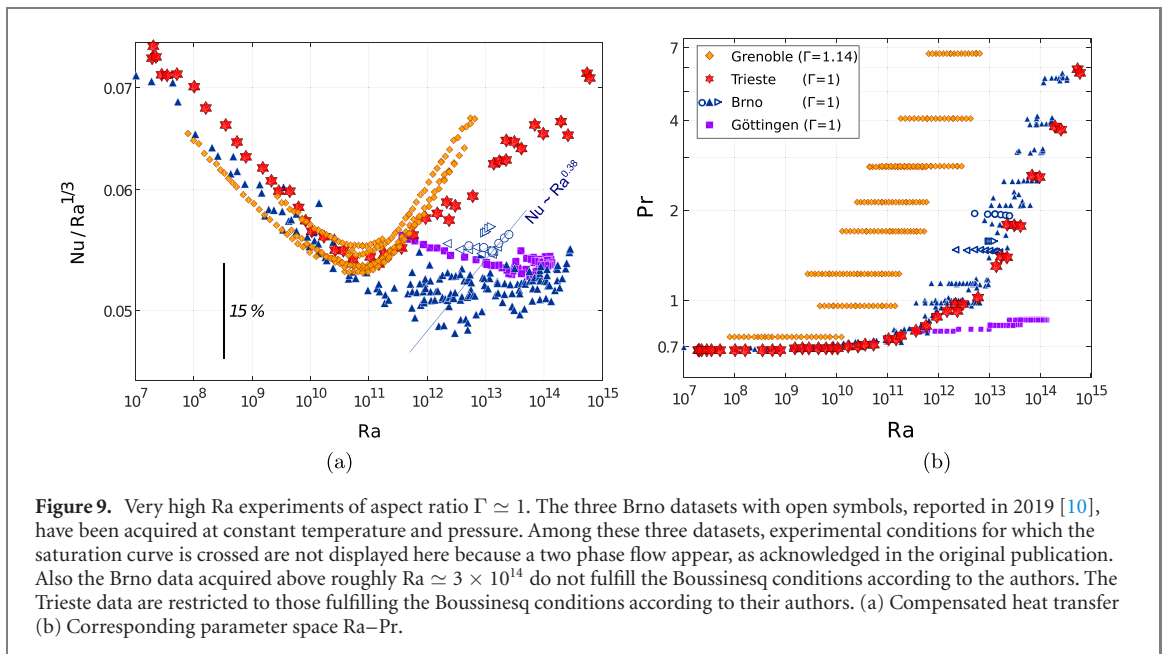

Figure 9. Very high Ra experiments of aspect ratio $\Gamma \simeq 1$. The three Brno datasets with open symbols, reported in 2019 [10], have been acquired at constant temperature and pressure. Among these three datasets, experimental conditions for which the saturation curve is crossed are not displayed here because a two phase flow appear, as acknowledged in the original publication. Also the Brno data acquired above roughly $Ra \simeq 3 \times 10^{14}$ do not fulfill the Boussinesq conditions according to the authors. The Trieste data are restricted to those fulfilling the Boussinesq conditions according to their authors. (a) Compensated heat transfer (b) Corresponding parameter space Ra–Pr.

figure 3 in [59] or figure 6(c) in [16]), and possibly in Brno 2019 data [10] (see figure 9(a)) can be interpreted as hindered transitions too. This calls for a direct exploration of the boundary layer flow in these experiments using alternative techniques such as fluctuations measurements.

Second, obviously a $Ra_U \sim \Gamma^{-3}$ (or $Ra_2^* \sim \Gamma^{-3}$) scaling cannot hold up to very large aspect ratio Γ, because it would have unphysical implications, eg that the sidewall confinement effect remain relevant for $\Phi \gg h$, and that the transition Ra could be significantly reduced. Therefore for large enough Γ, one expects the transition Ra to saturate at some constant value. The figure 8(b) plot suggests that the saturation occurs above $\Gamma \simeq 2-3$. This saturation supports our prediction that the characteristic length scale controlling the onset of the transition Rayleigh number in cylindrical cells is not the height h but rather $\mathcal{L} \sim \min(h, \Phi/2)$.

We conclude by listing three consequences of the model:

- Besides explaining the unexpected Γ dependence of the transitional Ra, the existence of *bl-eddies* could explain the observed great receptivity to sidewall details in confined cells ($\Gamma \lesssim 2$), because bl-eddies have a direct interaction with the sidewall. We therefore predict that sidewall receptivity of the transition to the ultimate regime will gradually vanish above $\Gamma \simeq 2-3$.

- The universal properties of *laterally-unconfined* ultimate state should be sought for $\Gamma \gtrsim 2-3$ typically. The Trieste $\Gamma = 4$ experiment suggests that an universal transition can be reach at Rayleigh number as low as $Ra_{\mathcal{L}} \simeq 2.10^{10}$ in laterally unconfined Rayleigh–Bénard cells, at similar Pr.

- From a practical point of view, a $\Gamma \simeq 2$ aspect ratio appears as a good compromise for the construction of new cells, as it maximizes the range of Ra where a transition can be observed with limited sidewall effects.

2.3. Conjecture#3: transition routes and the antagonistic properties of the wind

We still lack a phenomenological understanding for one important issue: some cells have pronounced heat transfer enhancement while others have not at similar Ra. This issue is illustrated on figure 9(a) with datasets of $\Gamma \simeq 1$ cells from Trieste, Grenoble, Göttingen and Brno (see figure 9(b) for the legend). Surely, it would be interesting to contribute to the debate on the interpretations of the Göttingen versus Brno datasets [7, 8, 10] in light of the present model, in particular on the evidences for and against the occurrence of a transition in both experiments. But the most striking issue to resolve is the difference between pronounced and/or early heat transfer enhancements (Grenoble and Trieste) and, on the another side, absent, hindered and/or late transitions (Brno and Göttingen). The same striking issue also exist for $\Gamma = 0.5$ cells, and the rest of this section is also relevant to these other geometries.
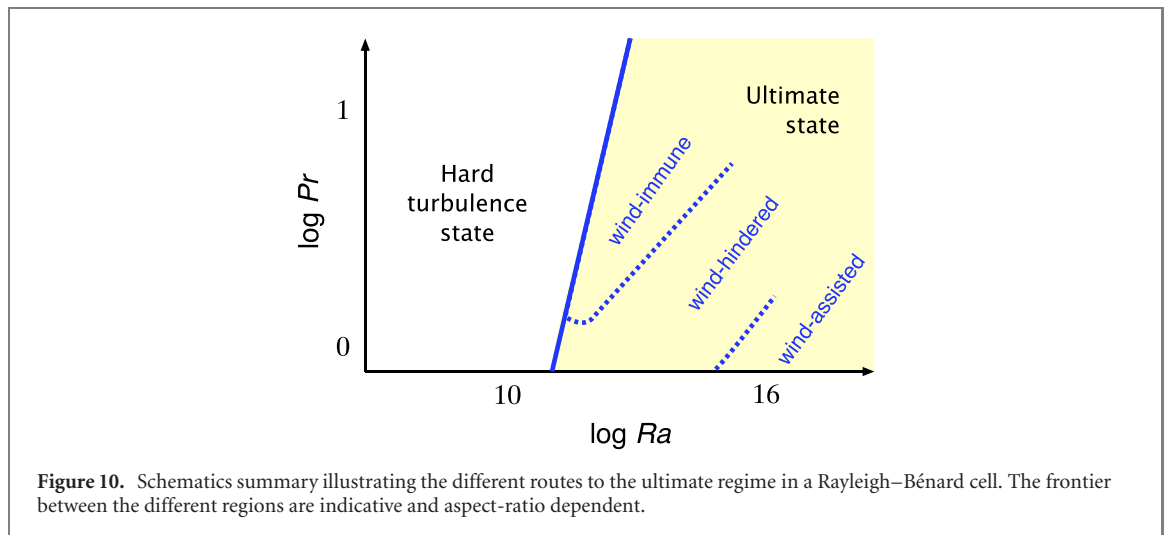
It is important to first stress that, rigorously speaking, almost no experiments discussed in the present work are in contradiction, because they are all obtained in different parts of the Ra–Pr parameter space (see figure 9(b) for $\Gamma \simeq 1$, and figure 6(a) from [16] for $\Gamma = 0.5$). In other word, there is no contradiction between all published data if one recall that the heat transfer Nu depends on three parameters: Ra, Pr and Γ. The only exception to this statement is the $\Gamma = 1$ datasets of Trieste and Brno, which roughly overlap along a curve in Ra–Pr space but significantly differ in heat transfer trend (see figure 9). This notable apparent contradiction may be a sign that the curve is close to a separation between two regions in Ra–Pr space, as developed below. Further dedicated investigation would be interesting, for instance by independent variation of Ra and Pr, as performed in Grenoble at lower Ra (see figure 9(b)).

In cells of large aspect ratio, the concept of large-scale wind is ill-defined (eg see [115–117]), and the wind can be seen a freely evolving large-scale vortical structure fulfilling our definition of a bl-eddy. In cell of finite aspect ratio (say for $\Gamma \lesssim 2$), the wind which settles across the cell is distinct from the freely evolving bl-eddies. This wind is topologically well constrained by the cell walls and it has its own space-time dynamics. We need to consider how the wind can alter the boundary layer and thus the conditions for a transition.

Our third conjecture is that the wind which settles across convection cells of finite aspect ratio can have antagonist effects of the strengthening of the bl-eddies, and therefore on the transition.

- A weak wind across the cell will not alter significantly the buoyant development of bl-eddies, and therefore will not alter their instability threshold. At a given Ra, the wind is known to weaken as Pr increases, at least in the range of parameters of interest of the present study [15, 113], with a dependence more or less consistent with the $Re \sim Pr^{-2/3}$ or $Re \sim Pr^{-5/7}$ scalings of the mixing length theories [59]. The Grenoble datasets are obtained at larger Pr than the others (eg. see figure 9(b)), and thus are most prone to be in this 'weak-wind limit'. Given the reported robustness of the critical Ra_U against variations of Re_{wind}, this weak-wind limit is most likely reached in Grenoble, and by analogy in Trieste. Surely, increasing Pr to infinity at constant Ra will inevitably restore, at some point, the stability of the boundary layer by reducing the bl-eddies Reynolds number $Re_{\mathcal{L}}$.

- An intermediate wind settling across a cell is expected to alter adversely the buoyant development of bl-eddies, and therefore to lead to an hindered or delayed transition. This prediction is based on evidences that a weakly forced flow over a thermally active laminar boundary layer lower heat transfer by disrupting the development of coherent plumes-like structures (eg. see [118–121] and reference within). At a given Ra, this intermediate case is expected to prevail at lower Pr (hence larger Re_{wind}). This is consistent with Ra–Pr parameter space of the Chicago, Eugene and Brno experiments, which all happen to exhibit scatter or irregularities of Nu(Ra) around $Ra = 10^{12}$ but no significant enhancement of Nu(Ra). The Göttingen experiment may as well be in this case below $Ra \simeq 10^{15}$.

- Finally, a high enough wind will inevitably destabilize the boundary layer and feed energy (back) into the bl-eddies. The Göttingen experiment may eventually reach this point at the largest Ra. It would be interesting to test this by varying Re_{wind} at given Ra.

A consequence of this third conjecture is the existence of different routes to the ultimate state in finite-Γ cells: wind-immune, wind-hindered and wind-assisted routes, as summarized by figure 10. This multiplicity of routes is reminiscent of classical boundary layers transition for which different paths to the turbulent state have also been identified [82, 86, 122]. Although the primary instability leading to the transition may differ between these routes, they lead to the same final ultimate state. One of the strongest experimental evidence supporting the existence of a single ultimate state is the common aspect-ratio dependence of the transition Ra reported in Grenoble, Göttingen and possibly in Trieste/Eugene cells.

Figure 10. Schematics summary illustrating the different routes to the ultimate regime in a Rayleigh–Bénard cell. The frontier between the different regions are indicative and aspect-ratio dependent.

3. Summary of the model

The motivation of this study was to sketch out a minimalist model able to reconcile all very high Rayleigh numbers experiments. A simple phenomenological model meeting this objective has been elaborated based on 3 conjectures, all directly elaborated from present knowledge of transitions in classical boundary layers:

- The transition is globally sub-critical, as depicted in figure 2(a), with well defined hard-turbulence and ultimate-state branches.

The heat transfer scaling exponent for the upper branch is around $\gamma \simeq 0.4$, consistently with Kraichnan prediction. The ultimate branch is reached only in few experiments. The non-universal cross-over between the two states is highly receptive to details of the cell, in particular from those coming from the lateral wall in small aspect ratio cells ($\Gamma < 2$).

- The boundary layer transition is associated with an instability of unsteady macroscopic structures, that we called boundary-layer eddies, or *bl-eddies*.

Wide and narrow cells should be differentiated, as depicted symbolically in figure 7. In wide cells (say for $\Gamma \gtrsim 3$), the *bl-eddies* typical size is set by the inter-plate distance (as in Trieste $\Gamma = 4$ cell). In narrow cells ($\Gamma \lesssim 2$), the *bl-eddies* typical size is set by the sidewall lateral confinement.

- The large-scale-circulation wind which settles in cells of finite aspect ratio can have antagonist effects on the boundary layer stability, resulting in 3 routes to the ultimate state (wind-immune, wind-hindered and wind-assisted), associated with different range of control parameters Ra, Pr and Γ, as illustrated on figure 10.

For a weak wind, the transition occurs when the $\mathrm{Re}_{\mathcal{L}}$ of *bl-eddies* reaches some threshold (Grenoble and Trieste cells). At smaller Pr and/or larger Ra, the wind strengthens and alters the dynamics of these eddies: the wind damps, prevents or delay the transition (Chicago, Eugene, Brno and Göttingen cells). Nevertheless, the shear from a strong enough wind will inevitably promote a transition again at high enough Ra (possibly in Göttingen).

Although mostly phenomenological, this model has testable predictions proposed through the text. It introduces a number of new ideas and concepts in the context of Rayleigh–Bénard convection, such as boundary layer *receptivity* of the transition, the adverse effect of wind on the transition, the existence of different routes to the ultimate state, the macroscopic length scale $\mathcal{L}$ and the resulting concept of laterally confined ($\Gamma \lesssim 2$) vs. unconfined ($\Gamma \gg 2$) ultimate state.

The existence of bl-eddies have been 'post-predicted' to reconcile experimental results, but we lack direct experimental or numerical evidence of their existence. Among the questions which remain open is how to discern the bl-eddies in DNS and visualization over an unsteady background flow.

Surely, the long history of studies on the transition of classical boundary layers, since Darcy, Hagen and Reynolds pipe experiments [81, 83–86, 123, 124] urges for circumspection and modesty when building a model of boundary layer transition. After more than one century of research, the threshold of the transition remains notoriously difficult to predict in pipe flows from the real world, and there is no reason why the Rayleigh–Bénard version of this transition, with lateral confinement and buoyancy, should be simpler. The present model is surely oversimplified, unfinished, and imperfect like existing models for the ultimate state. Nevertheless, it should be seen as a first attempt to propose an unifying and consistent picture

encompassing the diversity of results reported at very high Rayleigh numbers. Hopefully it can initiate the development of more refined models having a similar global perspective.

Acknowledgments

References

[1] Tritton D J 1988 *Physical Fluid Dynamics* 2nd edn (Oxford: Clarendon)
[2] Chillá F and Schumacher J 2012 New perspectives in turbulent Rayleigh–Bénard convection *Eur. Phys. J.* E **35** 58
[3] Kraichnan R 1962 Turbulent thermal convection at arbitrary Prandtl numbers *Phys. Fluids* **5** 1374
[4] Chavanne X, Chillá F, Castaing B, Hébral B, Chabaud B and Chaussy J 1997 Observation of the ultimate regime in Rayleigh–Bénard convection *Phys. Rev. Lett.* **79** 3648–51
[5] Sommeria J 1999 The elusive 'ultimate state' of thermal convection *Nature* **398** 294
[6] Chavanne X, Roche P-E, Chabaud B, Hébral B, Chillá F and Castaing B 2006 Comment on 'turbulent heat transport near critical points: non-Boussinesq effects' arXiv:cond-mat/0603262v1
[7] He X, Funfschilling D, Nobach H, Bodenschatz E and Ahlers G 2013 Comment on 'effect of boundary layers asymmetry on heat transfer efficiency in turbulent Rayleigh–Bénard convection at very high Rayleigh numbers' *Phys. Rev. Lett.* **110** 199401
[8] Urban P, Hanzelka P, Kralik T, Musilova V, Srnka A, Skrbek L, Urban *et al* 2013 reply: *Phys. Rev. Lett.* **110** 199402
[9] Weiss S, He X, Ahlers G, Bodenschatz E and Shishkina O 2018 Bulk temperature and heat transport in turbulent Rayleigh–Bénard convection of fluids with temperature-dependent properties *J. Fluid Mech.* **851** 374–90
[10] Urban P, Hanzelka P, Králík T, Macek M, Musilová V and Skrbek L 2019 Elusive transition to the ultimate regime of turbulent Rayleigh–Bénard convection *Phys. Rev.* E **99** 011101
[11] Zhu X, Mathai V, Stevens R J A M, Verzicco R and Lohse D Apr 2018 Transition to the ultimate regime in two-dimensional Rayleigh–Bénard convection *Phys. Rev. Lett.* **120** 144502
[12] Doering C R, Toppaladoddi S and Wettlaufer J S 2019 Absence of evidence for the ultimate regime in two-dimensional Rayleigh–Bénard convection *Phys. Rev. Lett.* **123** 259401
[13] Zhu X, Mathai V, Stevens R J A M, Verzicco R and Lohse D 2019 Reply to 'absence of evidence for the ultimate regime in two-dimensional Rayleigh–Bénard convection' *Phys. Rev. Lett.* (accepted 5 September 2019)
[14] Doering C R 2019 Absence of evidence for the 'ultimate' state of turbulent rayleigh–bénard convection arXiv:1909.10079
[15] Chavanne X, Chillá F, Chabaud B, Castaing B and Hébral B 2001 Turbulent Rayleigh–Bénard convection in gaseous and liquid He *Phys. Fluids* **13** 1300–20
[16] Roche P-E, Gauthier F, Kaiser R and Salort J 2010 On the triggering of the ultimate regime of convection *New J. Phys.* **12** 085014
[17] Gauthier F, Hébral B, Muzellier J and Roche P-E 2007 Ultimate regime of convection: search for a hidden triggering parameter *Advances in Turbulence XI* (Springer Proc. in Physics vol 117) ed J M L M Palma and A Silva Lopes (Berlin: Springer) p 645
[18] Wu X-Z 1991 Along a road to developed turbulence: free thermal convection in low temperature Helium gas *PhD Thesis* University of Chicago
[19] Niemela J J, Skrbek L, Sreenivasan K R and Donnelly R J 2000 Turbulent convection at very high Rayleigh numbers *Nature* **404** 837–40
[20] Niemela J J, Babuin S and Sreenivasan K R 2010 Turbulent rotating convection at high Rayleigh and taylor number *J. Fluid Mech.* **649** 509–22
[21] Niemela J J and Sreenivasan K R 2003 Confined turbulent convection *J. Fluid Mech.* **481** 355–84
[22] Niemela J J and Sreenivasan K R 2006 Turbulent convection at high Rayleigh numbers and aspect ratio 4 *J. Fluid Mech.* **557** 411–22
[23] Urban P, Hanzelka P, Musilová V, Králik T, La Mantia M, Srnka A and Skrbek L 2014 Heat transfer in cryogenic helium gas by turbulent Rayleigh–Bénard convection in a cylindrical cell of aspect ratio 1 *New J. Phys.* **16** 053042
[24] Bodenschatz E, He X, Van Gils D P M and Ahlers G 2015 Aspect-ratio dependence of the transition to the ultimate state of turbulent Rayleigh–Bénard convection *Proc. of the 15th European Turbulence Conf. (Delft, The Netherlands 25–28 August)*
[25] Ahlers G, Funfschilling D and Bodenschatz E 2009 Transitions in heat transport by turbulent convection at Rayleigh numbers up to 10^{15} *New J. Phys.* **11** 123001
[26] Ahlers G, He X, Funfschilling D and Bodenschatz E 2012 Heat transport by turbulent Rayleigh–Bénard convection for $\mathrm{Pr} \simeq 0.8$ and $3 \times 10^{12} \leqslant \mathrm{Ra} \leqslant 10^{15}$: aspect ratio $\Gamma = 0.50$ *New J. Phys.* **14** 103012
[27] He X, Funfschilling D, Bodenschatz E and Ahlers G 2012 Heat transport by turbulent Rayleigh–Bénard convection for $\mathrm{Pr} \simeq 0.8$ and $4 \times 10^{11} \leqslant \mathrm{Ra} \leqslant 2 \times 10^{14}$: ultimate-state transition for aspect ratio $\Gamma = 1.00$ *New J. Phys.* **14** 063030
[28] Grossmann S and Lohse D 2011 Multiple scaling in the ultimate regime of thermal convection *Phys. Fluids* **23** 045108
[29] Boussinesq J 1903 *Théorie analytique de la chaleur* (Paris: Gauthier-Villars)
[30] Castaing B, Gunaratne G, Heslot F, Kadanoff L, Libchaber A, Thomae S, Wu X-Z, Zaleski S and Zanetti G 1989 Scaling of hard thermal turbulence in Rayleigh–Bénard convection *J. Fluid Mech.* **204**
[31] Chaumat S, Castaing B and Chillá F Rayleigh–Bénard cells: influence of the plate properties *Advances in Turbulence IX, Proc. of the 9th European Turbulence Conf. (Southampton 2–5 July 2002)* pp 159–62
[32] Verzicco R 2003 Effects of nonperfect thermal sources in turbulent thermal convection *Phys. Fluids* **16** 1965
[33] Brown R, Nikolaenko A, Funfschilling D and Ahlers G 2005 Heat transport in turbulent Rayleigh–Bénard convection: Effect of finite top- and bottom-plate conductivities *Phys. Fluids* **17** 075108
[34] Wittenberg R W 2010 Bounds on Rayleigh–Bénard convection with imperfectly conducting plates *J. Fluid Mech.* **665** 158–98

[35] Roche P-E, Castaing B, Chabaud B, Hébral B and Sommeria J 2001 Side wall effects in Rayleigh Bénard experiments *Eur. Phys. J. B* **24** 405–8

[36] Ahlers G 2001 Effect of sidewall conductance on heat-transport measurements for turbulent Rayleigh–Bénard convection *Phys. Rev. E* **63** 015303(R)

[37] Verzicco R 2002 Side wall finite conductivity effects in confined turbulent thermal convection *J. Fluid Mech.* **473** 201–10

[38] Wu X-Z and Libchaber A 1992 Scaling relations in thermal turbulence: the aspect-ratio dependence *Phys. Rev. A* **45** 842

[39] Sun C, Ren L-Y, Song H and Xia K-Q 2005 Heat transport by turbulent convection in 1 m diameter cylindrical cells of widely varying aspect ratio *J. Fluid Mech.* **542** 165–74

[40] Nikolaenko A, Brown E, Funfschilling D and Ahlers G 2005 Heat transport by turbulent convection in cylindrical cells with aspect ratio one and less *J. Fluid Mech.* **523** 251–60

[41] Bailon-Cuba J, Emran M S and Schumacher J 2010 Aspect ratio dependence of heat transfer and large-scale flow in turbulent convection *J. Fluid Mech.* **665** 152

[42] Zhou Q, Liu B-F, Li C-M and Zhong B-C 2012 Aspect ratio dependence of heat transport by turbulent Rayleigh–Bénard convection in rectangular cells *J. Fluid Mech.* **710** 260–76

[43] du Puits R, Resagk C and Thess A 2013 Thermal boundary layers in turbulent Rayleigh–Bénard convection at aspect ratios between 1 and 9 *New J. Phys.* **15**

[44] Huang S-D and Xia K-Q 2016 Effects of geometric confinement in quasi-2-D turbulent Rayleigh–Bénard convection *J. Fluid Mech.* **794** 639–54

[45] Chillá F, Rastello M, Chaumat S and Castaing B 2004 Long relaxation times and tilt sensitivity in Rayleigh–Bénard turbulence *Eur. Phys. J. B* **40** 223–7

[46] Xi H-D and Xia K-Q 2008 Flow mode transitions in turbulent thermal convection *Phys. Fluids* **20** 055104

[47] Shishkina O and Horn S 2016 Thermal convection in inclined cylindrical containers *J. Fluid Mech.* **790**

[48] Mishra S C, Akhtar A and Garg A 2014 Numerical analysis of Rayleigh–Bénard convection with and without volumetric radiation *Numer. Heat Transfer* A **65** 144–64

[49] Sergent A, Xin S, Joubert P and Le Quere P 2006 Surface radiation effects on turbulent Rayleigh–Bénard convection in a parallelepipedic cavity *THMT-5 Conf.* (*Dubrovnik, Croatia*)

[50] Czarnota T and Wagner C 2016 Turbulent convection and thermal radiation in a cuboidal Rayleigh–Bénard cell with conductive plates *Int. J. Heat Fluid Flow* **57** 150–72

[51] du Puits R, Resagk C, Tilgner A, Busse F H and Thess A 2007 Structure of thermal boundary layers in turbulent Rayleigh–Bénard convection *J. Fluid Mech.* **572** 231–54

[52] Roche P-E, Castaing B, Chabaud B and Hébral B 2004 Heat transfer in turbulent Rayleigh–Bénard convection below the ultimate regime *J. Low Temp. Phys.* **134** 1011–42

[53] Stringano G and Verzicco R 2006 Mean flow structure in thermal convection in a cylindrical cell of aspect ratio one half *J. Fluid Mech.* **548** 1–16

[54] Weiss S and Ahlers G 2011 Turbulent Rayleigh–Bénard convection in a cylindrical container with aspect ratio gamma=0.50 and Prandtl number Pr=4.38 *J. Fluid Mech.* **676** 5–40

[55] Malkus W V R 1954 The heat transport and spectrum of thermal turbulence *Proc. R. Soc.* A **225** 196–212

[56] Howard L N 1966 Convection at high Rayleigh number *Applied Mechanics* ed G Henry (Berlin: Springer) pp 1109–15

[57] Siggia E D 1994 High Rayleigh number convection *Annu. Rev. Fluid Mech.* **26** 137–68

[58] Dubrulle B 2000 Scaling laws prediction from a solvable model of turbulent thermal convection *Europhys. Lett.* **51** 513–9

[59] Shraiman B I and Siggia E D 2000 Scalar turbulence *Nature* **405** 639–46

[60] Grossmann S and Lohse D 2000 Scaling in thermal convection: a unifying theory *J. Fluid Mech.* **407** 27–56

[61] Hölling M and Herwig H 2006 Asymptotic analysis of heat transfer in turbulent Rayleigh–Bénard convection *Int. J. Heat Mass Transfer* **49** 1129–36

[62] Waleffe F, Boonkasame A and Smith L M 2015 Heat transport by coherent Rayleigh–Bénard convection *Phys. Fluids* **27**

[63] Liu C-C 2017 Phenomenological Nusselt-Rayleigh scaling of turbulent thermal convection *J. Phys. Soc. Japan* **86** 123401

[64] Ching E S C, Dung O-Y and Shishkina O 2017 Fluctuating thermal boundary layers and heat transfer in turbulent Rayleigh–Bénard convection *J. Stat. Phys.* **167** 626–35

[65] Spiegel E A 1971 Convection in Stars I. Basic Boussinesq convection *Annu. Rev. Astron. Astrophys.* **9** 323–52

[66] Chavanne X 1997 Etude du régime turbulent en convection de Rayleigh–Bénard dans l'hélium liquide ou gazeux autour de 5 K *PhD Thesis* Université Joseph Fourier, Grenoble

[67] Roche P-E, Castaing B, Chabaud B and Hébral B 2001 Observation of the 1/2 power law in Rayleigh–Bénard convection *Phys. Rev. E* **63** 045303(R)

[68] Roche P-E, Gauthier F, Chabaud B and Bernard H 2005 Ultimate regime of convection: Robustness to poor thermal reservoirs *Phys. Fluids* **17** 5107

[69] Belmonte A, Tilgner A and Libchaber A 1994 Temperature and velocity boundary layers in turbulent convection *Phys. Rev. E* **50** 269

[70] Howard L N 1963 Heat transport by turbulent convection *J. Fluid Mech.* **17** 405

[71] Hassanzadeh P, Chini G P and Doering C R 2014 Wall to wall optimal transport *J. Fluid Mech.* **751** 627–62

[72] Fantuzzi G 2018 Bounds for Rayleigh–Bénard convection between free-slip boundaries with an imposed heat flux *J. Fluid Mech.* **837** R5

[73] Motoki S, Kawahara G and Shimizu M 2018 Maximal heat transfer between two parallel plates *J. Fluid Mech.* **851** R4

[74] Sun C and Xia K-Q 2005 Scaling of the Reynolds number on turbulent thermal convection *Phys. Rev. E* **72** 067302

[75] Salort J, Liot O, Rusaouen E, Seychelles F, Tisserand J-C, Creyssels M, Castaing B and Chilla F 2014 Thermal boundary layer near roughnesses in turbulent Rayleigh–Bénard convection: flow structure and multistability *Phys. Fluids* **26** 015112

[76] Goldstein R J and Tokuda S 1980 Heat transfer by thermal convection at high Rayleigh numbers *Int. J. Heat Transfer* **23** 738–40

[77] Wagner S, Shishkina O and Wagner C 2012 Boundary layers and wind in cylindrical Rayleigh–Bénard cells *J. Fluid Mech.* **697** 336–66

[78] Scheel J D and Schumacher J 2014 Local boundary layer scales in turbulent Rayleigh–Bénard convection *J. Fluid Mech.* **758** 344–73

[79] Kenjereš S and Hanjalić K 2002 Numerical insight into flow structure in ultraturbulent thermal convection *Phys. Rev. E* **66** 036307

[80] Morrison F A 2013 *An Introduction to Fluid Mechanics* (Cambridge: Cambridge University Press)

[81] Letellier C 2017 Intermittency as a transition to turbulence in pipes: A long tradition from Reynolds to the 21st century *C. R. Mec.* **345** 642–59

[82] Kachanov Y S 1994 Physical mechanisms of laminar-boundary-layer transition *Annu. Rev. Fluid. Mech.* **26** 411–82

[83] Schlichting H 2000 *Boundary-Layer Theory* 8th edn (New York: Springer)

[84] Pomeau Y 2015 The transition to turbulence in parallel flows: A personal view *C. R. Mec.* **343** 210–8

[85] Manneville P 2016 Transition to turbulence in wall-bounded flows: Where do we stand? *Mechanical Engineering Reviews* **3** 15–00684

[86] Barkley D 2016 Theoretical perspective on the route to turbulence in a pipe *J. Fluid Mech.* **803** P1

[87] Fraser C J, Higazy M G and Milne J S 1994 End-stage boundary layer transition models for engineering calculations *Proc. Inst. Mech. Eng.* C **208** 47–58

[88] Mckeon B J, Swanson C J, Zagarola M V, Donnelly R J and Smits A J 2004 Friction factors for smooth pipe flow *J. Fluid Mech.* **511** 41–4

[89] Verdoold J, Tummers M J and Hanjalić K 2009 Prime modes of fluid circulation in large-aspect-ratio turbulent Rayleigh–Bénard convection *Phys. Rev.* E **80** 037301

[90] Emran M S and Schumacher J 2015 Large-scale mean patterns in turbulent convection *J. Fluid Mech.* **776** 96–108

[91] Funfschilling D, Bodenschatz E and Ahlers G 2009 Search for the 'ultimate state' in turbulent Rayleigh–Bénard convection *Phys. Rev. Lett.* **103** 014503

[92] He X, Funfschilling D, Nobach H, Bodenschatz E and Ahlers G 2012 Transition to the ultimate state of turbulent Rayleigh–Bénard convection *Phys. Rev. Lett.* **108** 024502

[93] Kaiser R, Salort J and Roche P-E 2011 The ultimate regime of convection over uneven plates *J. Phys.: Conf. Ser.* **318** 052044

[94] Hagen G H L 1854 Über den einfluss der temperatur auf die bewegung des wassers in röhren *Druckerei der Königl* (Berlin: Akademie der Wissenschaften)

[95] Sackmann L A 1947 Hydraulique-sur les changements de regime dans les canalisations-mesures instantanees des caracteristiques *C. R. Hebd. Seances Acad. Sci.* **224** 793–5

[96] Gauthier F, Salort J, Bourgeois O, Garden J-L, du Puits R, Thess A and Roche P-E 2009 Transition on local temperature fluctuations in highly turbulent convection *Europhys. Lett.* **87** 44006

[97] He X, van Gils M, Bodenschatz D P E and Ahlers G 2014 Logarithmic spatial variations and universal f^{-1} power spectra of temperature fluctuations in turbulent Rayleigh–Bénard convection *Phys. Rev. Lett.* **112** 174501

[98] Gauthier F and Roche P-E 2008 Evidence of a boundary layer instability at very high Rayleigh number *Europhys. Lett.* **83** 24005

[99] von Rotta J 1956 Experimenteller beitrag zur entstehung turbulenter strömung im rohr *Arch. Appl. Mech.* **24** 258–81

[100] Landau L and Lifchitz E 1987 *Fluid Mechanics* 2nd edn (Oxford: Pergamon)

[101] Zocchi G, Moses E and Libchaber A July 1990 Coherent structures in turbulent convection, an experimental study *Physica* A **166** 387–407

[102] Puthenveettil B A and Arakeri J H 2005 Plume structure in high-Rayleigh-number convection *J. Fluid Mech.* **542** 217–49

[103] Zhou A, Sun C and Xia K-Q 2007 Morphological evolution of thermal plumes in turbulent Rayleigh–Bénard convection *Phys. Rev. Lett.* **98** 074501

[104] Shishkina O and Wagner C 2008 Analysis of sheet-like thermal plumes in turbulent Rayleigh–Bénard convection *J. Fluid Mech.* **599** 383–404

[105] Zhou A and Xia K-Q 2010 Physical and geometrical properties of thermal plumes in turbulent Rayleigh–Bénard convection *New J. Phys.* **12** 075006

[106] du Puits R and Willert C 2016 The evolution of the boundary layer in turbulent Rayleigh–Bénard convection in air *Phys. Fluids* **28**

[107] Parodi A, Von Hardenberg J, Passoni G, Provenzale A and Spiegel E A 2004 Clustering of plumes in turbulent convection *Phys. Rev. Lett.* **92** 194503

[108] Sakievich P J, Peet Y T and Adrian R J 2016 Large-scale thermal motions of turbulent Rayleigh–Bénard convection in a wide aspect-ratio cylindrical domain *Int. J. Heat Fluid Flow* **61** 183–96

[109] Xi H-D, Zhang Y-B, Hao J-T and Xia K-Q 2016 Higher-order flow modes in turbulent Rayleigh–Bénard convection *J. Fluid Mech.* **805** 31–51

[110] du Puits R, Resagk C and Thess A 2007 Breakdown of wind in turbulent thermal convection *Phys. Rev.* E **75** 016302

[111] Podvin B and Sergent A 2012 Proper orthogonal decomposition investigation of turbulent Rayleigh–Bénard convection in a rectangular cavity *Phys. Fluids* **24** 105106

[112] He X, van Gils D P M, Bodenschatz E and Ahlers G 2015 Reynolds numbers and the elliptic approximation near the ultimate state of turbulent Rayleigh–Bénard convection *New J. Phys.* **17** 063028

[113] Musilová V, Králík T, La Mantia M, Macek M, Urban P and Skrbek L 2017 Reynolds number scaling in cryogenic turbulent Rayleigh–Bénard convection in a cylindrical aspect ratio one cell *J. Fluid Mech.* **832** 721–44

[114] Barkley D and Tuckerman L S 2007 Mean flow of turbulent–laminar patterns in plane Couette flow *J. Fluid Mech.* **576** 109–37

[115] van Reeuwijk M, Jonker H J J and Hanjalic K 2005 Identification of the wind in Rayleigh–Bénard convection *Phys. Fluids* **17** 051704

[116] Pandey A, Scheel J D and Schumacher J 2018 Turbulent superstructures in Rayleigh–Bénard convection *Nat. Commun.* **9** 2118

[117] Stevens R J A M, Blass A, Zhu X, Verzicco R and Lohse D 2018 Turbulent thermal superstructures in Rayleigh–Bénard convection *Phys. Rev. Fluids* **3** 041501

[118] Andrzej Domaradzki J and Metcalfe R W 1988 Direct numerical simulations of the effects of shear on turbulent Rayleigh–Bénard convection *J. Fluid Mech.* **193** 499–531

[119] Scagliarini A, Gylfason A and Toschi F 2014 Heat-flux scaling in turbulent Rayleigh–Bénard convection with an imposed longitudinal wind *Phys. Rev.* E **89** 043012

[120] Shevkar P P, Gunasegarane G S, Mohanan S K and Puthenveettil B A 2019 Effect of shear on coherent structures in turbulent convection *Phys. Rev. Fluids* **4** 043502

[121] Blass A, Zhu X, Verzicco R, Lohse D and Stevens R J A M 2019 Flow organization and heat transfer in turbulent wall sheared thermal convection arXiv:1904.11400(physics.flu-dyn

[122] Henningson D S and Schmid P J 2001 *Stability and Transition in Shear Flows* 1st edn vol 142 (New York: Springer)

[123] Huerre P and Rossi M 1998 *Hydrodynamic Instabilities in Open Flows* (Cambridge: Cambridge University Press) pp 81–294

[124] Eckert M 2010 The troublesome birth of hydrodynamic stability theory: Sommerfeld and the turbulence problem *Eur. Phys. J.* H **35** 29–51

[125] Bouillaut V, Lepot S, Aumaître S and Gallet B 2019 Transition to the ultimate regime in a radiatively driven convection experiment *J. Fluid Mech.* **861** R5

[126] Prasanna S and Venkateshan S P 2014 Convection induced by radiative cooling of a layer of participating medium *Phys. Fluids* **26** 056603

[127] van Reeuwijk M, Jonker H J J and Hanjalić K 2008 Wind and boundary layers in Rayleigh–Bénard convection. II. Boundary layer character and scaling *Phys. Rev.* E **77** 036312

[128] du Puits R, Li L, Resagk C, Thess A and Willert C 2014 Turbulent boundary layer in high Rayleigh number convection in air *Phys. Rev. Lett.* **112** 124301

[129] Shen Y, Tong P and Xia K-Q 1996 Turbulent convection over rough surfaces *Phys. Rev. Lett.* **76** 908–11

[130] Ciliberto S and Laroche C 1999 Random roughness of boundary increases the turbulent scaling exponent *Phys. Rev. Lett.* **82** 3998–4001